Modeling of PAHs From Global to Regional Scales: Model Development (IAP-AACM_PAH v1.0) and Investigation of Health Risks in 2013 and 2018 in China

Zichen Wu[1,2,3], Xueshun Chen[1,2,3]*, Zifa Wang[1,2,3]*, Huansheng Chen[1,2,3], Zhe Wang[1,2,3], Qing Mu[4], Lin Wu[1,2,3], Wending Wang[1,2,3], Xiao Tang[1,2,3], Jie Li[1,2,3], Ying Li[1,2,3], Qizhong Wu[5], Yang Wang[3,6], Zhiyin Zou[1,2,3], Zijian Jiang[1,2,3]

[1] State Key Laboratory of Atmospheric Boundary Layer Physics and Atmospheric Chemistry, Institute of Atmospheric Physics, Chinese Academy of Sciences, Beijing 100029, China

[2] Key Laboratory of Atmospheric Environment and Extreme Meteorology, Institute of Atmospheric Physics, Chinese Academy of Sciences, Beijing 100029, China

[3] University of Chinese Academy of Sciences, Beijing 100049, China

[4] Department of Health and Environmental Sciences, School of Science, Xi'an Jiaotong-Liverpool University, Suzhou 215123, China

[5] Beijing Normal University, Beijing 100875, China

[6] Research Center for Eco-Environmental Sciences, Chinese Academy of Sciences, Beijing 100085, China

Correspondence to: Xueshun Chen (chenxsh@mail.iap.ac.cn) and Zifa Wang (zifawang@mail.iap.ac.cn)

Abstract. Polycyclic aromatic hydrocarbons (PAHs) significantly impact human health due to their persistence, toxicity, and potential carcinogenicity. Their global distribution and regional changes caused by emission changes, especially over areas in developing countries, remain to be understood along with their health impacts. This study implemented a PAH module in the global-regional nested Atmospheric Aerosol and Chemistry Model (IAP-AACM) to investigate the global distribution of PAHs and the change in their health risks from 2013 to 2018 in China. An evaluation against observations showed that the model could capture well the spatial distribution and seasonal variation of Benzo[a]pyrene (BaP), the typical indicator species of PAHs. At a global scale, the annual mean concentrations are highest in China, followed by Europe and India, with high values exceeding the target values of 1 ng m^{-3} over some areas. Compared with 2013, the concentration of BaP in China decreased in 2018 due to emission reductions, whereas it increased in India and Southern Africa. However, the decline is much smaller than for PM$_{2.5}$ during the same period. The concentration of BaP decreased by 8.5% in Beijing-Tianjin-Hebei (BTH) and 9.4% in the Yangtze River Delta (YRD). It even increased over areas in the Sichuan Basin due to changes in meteorological conditions. The total incremental lifetime cancer risk (ILCR) posed by BaP

only showed a slight decrease in 2018 and the population in East China still faced significant potential health risks. The results indicate that strict additional control measures should be taken to reduce the pollution and health risks of PAHs effectively. The study also highlights the importance of considering changes in meteorological conditions when evaluating emission changes from concentration monitoring.

1 Introduction

Polycyclic aromatic hydrocarbons (PAHs) are aromatic compounds with two or more aromatic rings. PAHs have been categorized as persistent organic pollutants (POPs) by the United Nations Economic Commission for Europe's (UNECE's) Convention on Long-Range Transboundary Air Pollution (CLRTAP) (Friedman and Selin, 2012), and they are widely distributed in the environment through atmospheric transport. PAHs have attracted significant attention in environmental research and risk assessment due to their persistence, toxicity, and potential carcinogenicity (Chen and Liao, 2006; Shen et al., 2014). These compounds are generated from both natural and anthropogenic sources (Haritash and Kaushik, 2009). Volcanic eruption, forest, and prairie fire are the major natural sources of atmospheric PAHs (Baek et al., 1991). Anthropogenic sources are the most important source of PAHs, including incomplete combustion of fossil fuels and biomass (Li et al., 2022; Ravindra et al., 2008).

Understanding the sources, distribution, and fate of PAHs is crucial for assessing their impacts on human health and the environment. Upon emission into the atmosphere, PAHs are redistributed by gas-particulate partitioning, gaseous-phase reactions, heterogeneous reactions, air-soil exchange, and wet/dry deposition during long-range transport (LRT, Inomata et al., 2013). Monitoring is the most commonly used way to investigate the concentration of PAHs in the atmosphere. Due to the high costs of observation and technical limitations, it is difficult to conduct a long-term and broad regional analysis through monitoring (Zhen, 2023). Up to now, there are few continuous observations over the major continents at the same time (Dong et al., 2023). A transport model is an effective tool to simulate the distribution of PAHs and their LRT, which can greatly enhance our understanding of the distribution of PAHs on a regional and global scale (Byun and Schere, 2006; Wang et al., 2021).

As recently outlined by Galarneau et al. (2014), several numerical modeling studies have been reported in the literature. The models that can simulate PAHs include but are not limited to the following examples, GEOS-Chem (Friedman et al., 2014; Friedman and Selin, 2012), ECHAM5 (Lammel and

60   Sehili, 2007; Lammel et al., 2009; Lammel et al., 2015; Octaviani et al., 2019), CAM5 (Lou et al., 2023;

61   Shrivastava et al., 2017), and MOZART-4 (Shen et al., 2014). The horizontal resolutions of these reported

62   models are primarily at $4° \times 5°$ and $2.8° \times 2.8°$. Shen et al. (2014) simulated the transport of

63   Benzo[a]pyrene (BaP), one of the most toxic and highly carcinogenic PAHs, in the global troposphere

64   based on MOZART-4, and they showed that the model resolution was crucial for the health risks

65   assessment. Lammel et al. (2015) demonstrated the significant impact of gas-particle partitioning

66   mechanisms on the atmospheric lifetime, compartment distributions, and LRT of PAHs. The regional

67   modeling studies focusing on Europe, East Asia, and North America have also been reported, with

68   horizontal resolutions ranging mainly from 54 km×54 km to 24 km×24 km (CMAQ (Aulinger et al.,

69   2009; Aulinger et al., 2007; Bieser et al., 2012; San José et al., 2013; Efstathiou et al., 2016), WRF-Chem

70   (Mu et al., 2018), AURAMS (Galarneau et al., 2014), and CanMETO (Zhang et al., 2011a; Zhang et al.,

71   2011b; Zhang et al., 2009)). Efstathiou et al. (2016) showed that considering absorption and adsorption

72   processes can better capture the concentration levels and seasonal variations of BaP. In recent years, the

73   effect of the heterogeneous reaction process of PAHs on transportation has also been studied. Mu et al.

74   (2018) developed a new kinetic scheme describing the effects of temperature and humidity on the organic

75   aerosol coating of BaP and BaP reaction rate. They found that low temperature and low humidity can

76   significantly increase the lifetime of BaP and enhance its LRT capacity.

77   However, the resolutions and spatial range differed greatly between these models. Most of the

78   models are either global or regional. There is a lack of simulation studies focusing on both global and

79   key regions, making it difficult to investigate a specific focus in a global background in a consistent

80   manner. Additionally, the resolution of most global models is low, which will further affect the health

81   risk assessment of PAHs. Furthermore, the up-to-date mechanisms (gas-particle partitioning,

82   heterogeneous reaction, and air-soil exchange) established for PAHs simulations are not considered in

83   earlier modeling studies.

84   China is one of the largest PAH-emitting countries in the world (Inomata et al., 2012; Zhang and

85   Tao, 2009). High concentrations of BaP have been reported (Bieser et al., 2012; Liu et al., 2014;

86   Shrivastava et al., 2017; Su et al., 2023). Over the polluted regions in eastern China, annual

87   concentrations of BaP exceeded 1 ng m^{-3}, the target values proposed in the European Union (EU) and

88   China. To improve air quality and protect public health, the State Council of China promulgated "the

Action Plan on Air Pollution Prevention and Control" (the Action Plan) in 2013. This Action Plan established many effective emission reduction and energy-saving policies, such as strengthening industrial emission standards, eliminating outdated polluting industries, upgrading industrial boilers, and developing clean fuels in the residential sector. Since then, many studies have investigated the changes in concentration levels and health risks of conventional pollutants, such as $PM_{2.5}$ (Feng et al., 2019; Wang et al., 2018; Zhang et al., 2019; Zhu et al., 2021; Wang et al., 2019). Wang et al. (2019) pointed out that the annual average concentrations of $PM_{2.5}$ in the Beijing-Tianjin-Hebei (BTH), the Yangtze River Delta (YRD), and the Pearl River Delta (PRD) all decreased by more than 27% in 2017, indicating that the control measures have achieved remarkable effects and the air quality has been significantly improved. However, for non-conventional pollutants, such as BaP and other PAHs, their concentration changes due to emission reduction in China after implementing of policies have not been quantified. The changes in health risks and the benefits from control measures were not yet assessed.

Considering the aforementioned, we simulated PAHs from global to regional scales by coupling the key physical and chemical modules associated with PAHs in a global-regional nested atmospheric transport model. In particular, newly established parametrizations of gas-particle partitioning and heterogeneous reaction were incorporated into the model. Then the changes in global concentration and health risks of BaP over China were quantified based on model evaluation against a collected observation dataset. The study can advance our understanding of global PAHs distribution and regional health risks and their responses to emission change. The paper is arranged as follows: Section 2 briefly describes the host model (IAP-AACM), the physical and chemical modules related to PAHs, and the method of assessing health risks. Section 3 presents the configuration of the model and the observations used in the evaluation. Section 4 shows the global and regional distributions of BaP concentrations and analyzes the health risks associated with BaP in China. Section 5 discusses the uncertainty of the model. In Sect. 6, the main conclusions are summarized.

2 Model description and development

2.1 Description of host model

The model used in this study is the Atmospheric Aerosol and Chemistry Model developed by the Institute of Atmospheric Physics, Chinese Academy of Sciences (IAP-AACM) (Wei et al., 2019), which

117 was developed based on the Global Nested Air Quality Prediction Modeling System (GNAQPMS, Chen

118 et al., 2015; Wang et al., 2001). IAP-AACM is a 3-D Eulerian transport model that uses a multi-scale

119 domain-nesting approach to simulate atmospheric chemistry and aerosol processes from global to

120 regional scales. As recently described by Chen et al. (2015), compared with the traditional multi-scale

121 modeling methods (Seigneur et al., 2001), the online nesting method uses the same parameters in the

122 global and regional domains, which avoids uncertainties caused by different boundary conditions, and it

123 also provides boundary conditions at higher time resolution (Zhang et al., 2012b; Chen et al., 2015), thus

124 improving the performance of the model at the regional scale.

125 This model includes emission, horizontal and vertical advection (Walcek and Aleksic, 1998),

126 diffusion (Byun and Dennis, 1995), dry deposition (Zhang et al., 2003), gaseous chemistry (CBM-Z,

127 Carbon Bond Mechanism version Z, Zaveri and Peters, 1999), heterogeneous chemistry (Li et al., 2012),

128 aqueous reactions in clouds, and wet scavenging (Stockwell et al., 1990). It has been successfully and

129 widely applied to simulate the spatial-temporal distribution characteristics of gaseous pollutants, aerosol

130 components, and the long-distance transportation of mercury (Chen et al., 2015; Chen et al., 2014; Wei

131 et al., 2019; Ye et al., 2021; Du et al., 2019). In addition, advanced particle microphysics (APM) has been

132 incorporated to simulate new particle formation processes and predict the particle number concentrations

133 at global and regional scales (Chen et al., 2021).

2.2 Development of the PAH module

135 The PAH processes in the IAP-AACM model include gaseous-phase reaction, heterogeneous

136 reaction, gas-particle partitioning, air-soil exchange, dry deposition, and wet scavenging. The simulated

137 species include BaP, Benzo[b]fluorathene (BbF), Benzo[k]fluorathene (BkF), and Indeno[1,2,3-

138 cd]pyrene (IcdP) in the gas and particulate phases (Wu et al., 2024). In this study, we mainly focus on

139 BaP due to its highly carcinogenic nature and the relatively rich observations.

2.2.1 Gaseous-phase reactions

141 PAHs are degraded through reactions with various atmospheric oxidants such as hydroxyl radical

142 (OH), nitrate radical (NO_3), and ozone (O_3) in the troposphere (Lammel and Sehili, 2007). Among these

143 oxidants, the reactions with OH are considered to be the most important pathway for the removal of

144 PAHs. The nighttime reaction of PAHs with NO_3 is also important in the atmosphere (Keyte et al., 2013).

145   Therefore, reactions of gaseous-phase BaP with OH, NO_3, and O_3 are all considered in the model. The

146   second-order rate coefficients are 5.0×10^{-11}, 5.4×10^{-11}, and 2.6×10^{-17} cm^3 molecules^{-1} s^{-1}, respectively

147   (Inomata et al., 2013; Finlayson-Pitts and Pitts, 2000; Klöpffer et al., 2007).

2.2.2 Heterogeneous reaction

149   In the case of BaP, the heterogeneous reaction with O_3 is considered to be the dominant loss

150   (Finlayson‐Pitts and Pitts, 2000; Efstathiou et al., 2016). Studies have shown that the process of

151   heterogeneous reaction can be well described by the Langmuir-Hinshelwood mechanism (Kahan et al.,

152   2006; Kwamena et al., 2007), in which BaP is adsorbed to the surface while the O_3 is in phase equilibrium.

153   The first-order reaction rate coefficient k (s^{-1}) of the Langmuir-Hinshelwood mechanism is as follows:

$$k = \frac{k_{max} K_{O_3} [O_3]}{1 + K_{O_3} [O_3]} \tag{1}$$

$$\frac{\partial C}{\partial t} = -K_{O_3} [O_3] \tag{2}$$

154   Where k_{max} is the maximum rate coefficient, and the value is 0.060 ± 0.018 s^{-1}. $[O_3]$ is the

155   concentration of O_3 (mol cm^{-3}). K_{O_3} is the O_3 to surface equilibrium constant ($0.028\pm0.014\times10^{-13}$ cm^3).

156   In addition, we incorporated a more detailed parameterization (ROI-T) developed by Mu et al. (2018)

157   based on the Langmuir-Hinshelwood mechanism. The scheme emphasizes the importance of

158   representing the dependence of degradation on temperature and humidity, when coated by organic

159   aerosols The first-order reaction rate coefficient k (s^{-1}) is given by Eq. (3).

$$k = base + \frac{max - base}{1 + (\frac{xhalf}{[O_3]})^{rate}} \tag{3}$$

160   Where $base$, max, $rate$, and $xhalf$ are all the parameterizations of the heterogeneous reaction,

161   with specific values shown in Mu et al. (2018). In our study, we coupled these two parameterizations as

162   two options for O_3 degradation by heterogeneous reaction in IAP-AACM. The model results using these

163   two schemes were compared to analyze the influence of heterogeneous reaction schemes on BaP

164   concentration. The ROI-T scheme was used as the default in this study.

2.2.3 Gas-particle partitioning

166   The partition of compounds between the gas and particulate phases is parameterized with the gas-

167   particle partitioning coefficient (K_P, m^3 μg^{-1}) (Harner and Bidleman, 1998):

$$K_P = (\frac{[PAH]\_p}{[TSP]})/[PAH]\_g \qquad (4)$$

Where $[PAH]\_g$ and $[PAH]\_p$ are the concentrations of PAHs in the gas and particulate phase ($\mu g\ m^{-3}$), and $[TSP]$ is the concentration of total suspended particles (TSP, $\mu g\ m^{-3}$) in the atmosphere ($\mu g\ m^{-3}$).

Adsorption onto black carbon (BC) and absorption into aerosol organic matter (OM) are two important mechanisms of gas-particle partitioning (Odabasi et al., 2006). Therefore, we use the gas-particle partition coefficient equation to represent these two mechanisms, which was derived by Dachs and Eisenreich, 2000:

$$K_P = \left[\frac{(f_{OM}MW_{OCT}\delta_{OCT})K_{OA}}{(\rho_{OCT}MW_{OM}\delta_{OM}10^{12})}\right] + [\left(\frac{f_{BC}a_{BC}K_{SA}}{a_{AC}10^{12}}\right)] \qquad (5)$$

Where MW_{OCT} and MW_{OM} are the mean molecular weights of octanol and OM phase (g mol^{-1}), δ_{OCT} and δ_{OM} are the activity coefficient of the absorbing compound in octanol and OM phase, respectively. f_{OM} and f_{BC} are the mass fractions of OM phase on TSP and the BC in the aerosol. ρ_{OCT} is the density of octanol (0.820 kg L^{-1}). a_{BC} and a_{AC} are the specific surface areas of BC (62.7 m^2 g^{-1}, Jonker and Koelmans, 2002) and activated carbon (AC), respectively. In this study, we use the same assumption as Odabasi et al. (2006) ($MW_{OCT}/MW_{OM} = 1$,$\delta_{OCT}/\delta_{OM} = 1$, and $a_{BC}/a_{AC} = 1$).

$$logK_{OA} = A + B/(T) \qquad (6)$$

Where K_{OA} is the octanol–air partitioning coefficient (temperature dependent). T is the temperature (K). The values of A and B are 5382 and -6.5, respectively (Odabasi et al., 2006).

$$logP_L = m_L(T)^{-1} + b_L \qquad (7)$$

$$logK_{SA} = -0.85logP_L + 8.94 - \log\left(\frac{998}{a_{BC}}\right) \qquad (8)$$

Where P_L is the supercooled liquid vapor pressure (Pa). The values of b_L and m_L are 12.59 and -5252, respectively (Dachs and Eisenreich, 2000). K_{SA} is the soot–air partitioning coefficient (L kg^{-1}), which is a function of P_L and a_{BC} (van Noort, 2003).

2.2.4 Air-soil exchange

The semi-volatility and persistence of PAHs allow them to dynamically exchange between the atmosphere and soil by deposition and re-volatilization from ground surfaces (Semeena and Lammel, 2005). These processes can affect the distribution and long-distance transport of PAHs in the environment. As described by Hansen et al. (2004), air–soil exchange is parameterized following Strand and Hov

191 (1996), which is based on Jury et al. (1983). Here, soil (standard soil) is considered to be a homogeneous

192 layer of thickness z_s= 0.15 m, and standard values and chemical properties are provided by Jury et al.

193 (1983) (Table S1). The differential equation for the change of concentrations in soil and air can be

194 expressed by Eq. (9) and Eq. (10):

$$\frac{\partial c_s}{\partial t} = \frac{1}{z_s}\left(F_{exc,soil} + F_{wet}\right) - k_{soil}c_s \tag{9}$$

$$\frac{\partial c_a}{\partial t} = -\frac{1}{z_a}F_{exc,soil} \tag{10}$$

195 Where C_a and C_s are the concentrations of PAHs in the atmosphere and soil, respectively. The z_a

196 is the lowest atmospheric layer depths (m), F_{wet} is the wet deposition flux (mol s^{-1} m^{-2}). k_{soil} is the

197 degradation rate in soil, which is estimated to be 2.2×10^{-8} s^{-1} (Finlayson‐Pitts and Pitts, 2000; Klöpffer

198 et al., 2007; Lammel et al., 2009). The air–soil exchange flux ($F_{exc,soil}$) is given by Eq. (11):

$$F_{exc,soil} = K_{a/s}(c_a - \frac{C_s}{K_{soil-air}}) \tag{11}$$

199 $K_{soil-air}$ is the partitioning coefficient between soil and air, which is given by Karickhoff (1981):

$$K_{soil-air} = 4.11 \times 10^{-4} \times \rho_s f_{oc} K_{OA} \tag{12}$$

200 Where f_{OC} is the fraction of OC in soil and 4.11×10^{-4} is a constant with units of m^3 kg^{-1}. ρ_s is the

201 density of soil. $K_{a/s}$ is the overall exchange velocity (m s^{-1}), which can be estimated by Eq. (13) (Strand

202 and Hov, 1996):

$$K_{a/s} = \frac{D_G^{air} a^{10/3}(1 - l - a)^{-2} + D_L^{water} l^{10/3} K_{WA}(1 - l - a)^{-2}}{z_s/2} \tag{13}$$

203 Where D_G^{air} and D_L^{water} are the air and liquid diffusion coefficient (m^2 s^{-1}), respectively. K_{WA} is

204 the water-air partitioning coefficient. The differential equation is solved the ODEPACK

205 (https://github.com/jacobwilliams/odepack).

206 **2.2.5 Dry and wet deposition**

207 PAHs can be removed from the atmosphere and enter terrestrial ecosystems through dry and wet

208 deposition (Cao et al., 2021). Dry deposition and wet scavenging have been included in IAP-AACM. For

209 the gaseous species of PAHs, their wet scavenging is assumed to be the same as xylene in the CBMZ

210 mechanism, which is also an aromatic hydrocarbon like BaP; for the PAHs in the particle phase, these

211 two processes are treated similarly to that of organic aerosol.

2.3 Risk assessment

The incremental lifetime cancer risk (ILCR) is widely used to calculate the risk of human exposure to PAHs (Nam et al., 2021). The carcinogenic risk of PAHs to humans through different exposure routes was calculated based on the health risk evaluation model proposed by the U.S. Environmental Protection Agency (EPA) (Smith et al., 1999).

The national population data at 1 km×1 km (at the Equator) resolution in 2013 and 2018 were obtained from the LandScan (Oak Ridge National Laboratory; database can be accessed via: https://landscan.ornl.gov, last access: 20 January 2024) and re-gridded to 1°× 1° and 0.33°× 0.33° to match the model resolution.

2.3.1 Daily exposure dose

Dermal contact and inhalation are regarded as the major routes of human exposure to BaP (Li et al., 2010; Ma et al., 2020; Zhang et al., 2016). In this study, the health risk for the entire population and three groups (adult women, adult men, and children) are calculated. The daily exposure dose (ADD) to PAHs through the two exposure routes is calculated as follows:

$$ADD_{der} = \frac{C \times SA \times ABS \times AF \times EF \times ED}{AT \times BW} \tag{14}$$

$$ADD_{inh} = \frac{C \times IR \times EF \times ED}{AT \times BW} \tag{15}$$

Where ADD_{der} and ADD_{inh} are the average daily exposure dose that enters the body through the dermal contact and inhalation, respectively (ng kg^{-1} day^{-1}), C is the concentration of PAHs (ng m^{-3}). IR is the inhalation rate (m^3 d^{-1}). AF is the dermal adherence rate (mg cm^{-2} d^{-1}). EF and ED are the exposure duration (d a^{-1}) and period (a), respectively. BW is the body weight (kg). SA is the skin exposed surface area (cm^2). ABS is the skin absorption factor. AT is the average exposure time (d). The values are shown in Table S2.

2.3.2. Incremental lifetime cancer risk (ILCR)

The ILCR was calculated based on the ADD:

$$ILCR_{der} = ADD_{der} \times SFO_{der} \times CF \tag{16}$$

$$ILCR_{inh} = ADD_{inh} \times SFO_{inh} \times CF \tag{17}$$

$$TILCR = ILCR_{der} + ILCR_{inh} \tag{18}$$

234   Where $ILCR_{der}$ and $ILCR_{inh}$ are lifetime cancer risks through the dermal contact and inhalation,

235   respectively. $TILCR$ is the total lifetime cancer risk of exposure through the two pathways. SFO is a

236   cancer slope factor (kg day mg^{-1}) and CF is the conversion factor. The values are shown in Table S2.

237   For carcinogen, an $ILCR$ less than 1×10^{-6} indicates negligible cancer risk, an $ILCR$ between 1×10^{-6}

238   and 1×10^{-4} indicates potential cancer risk, and an $ILCR$ larger than 1×10^{-4} indicates high potential

239   cancer risk.

240   **3 Experiments setup and observation data**

241   **3.1 Experiments setup**

242   In this study, we used two nested domains covering the whole globe and East Asia as shown in Fig.

243   S1. The horizontal resolutions are $1° \times 1°$ and $0.33° \times 0.33°$, respectively. A total of 20 vertical layers are

244   used in IAP-AACM. The first layer of the model is approximately 50 m deep and the top layer extends

245   to 20 km. The simulation results from January 1st to December 31st 2013 and from January 1st to

246   December 31st 2018 were used for analysis. Each simulation had a one-month spin-up before January 1st

247   to reduce the influence of initial conditions. The global version of the Weather Research and Forecasting

248   model (WRF, version 3.7.1) (Zhang et al., 2012a; Skamarock et al., 2008) provides the meteorological

249   fields to drive the IAP-AACM. The initial and boundary conditions of the global WRF were produced

250   by Final Analysis data (FNL) from the National Centers for Environmental Prediction (NCEP).

251   The emission inventory of BaP in 2013 and 2018 was derived from the Emissions Database for

252   Global   Atmospheric   Research   (EDGAR,   Crippa   et   al.,   2020,   available   from

253   https://edgar.jrc.ec.europa.eu/dataset_pop60#sources, last access: 15 December 2023). We mainly

254   analyzed the results using EDGAR emission, which mainly includes anthropogenic sources such as

255   power, transportation, industrial, agricultural, and energy for buildings. An additional simulation for 2013

256   using the emission inventory developed by the research group of Peking University (PKU)

257   (http://inventory.pku.edu.cn, last access: 10 February 2023) was used to investigate the uncertainties

258   from emissions. The resolution of both emission inventories is $0.1° \times 0.1°$. Therefore, we re-gridded the

259   emissions inventories to match the model grids at $1° \times 1°$ and $0.33° \times 0.33°$ resolution.
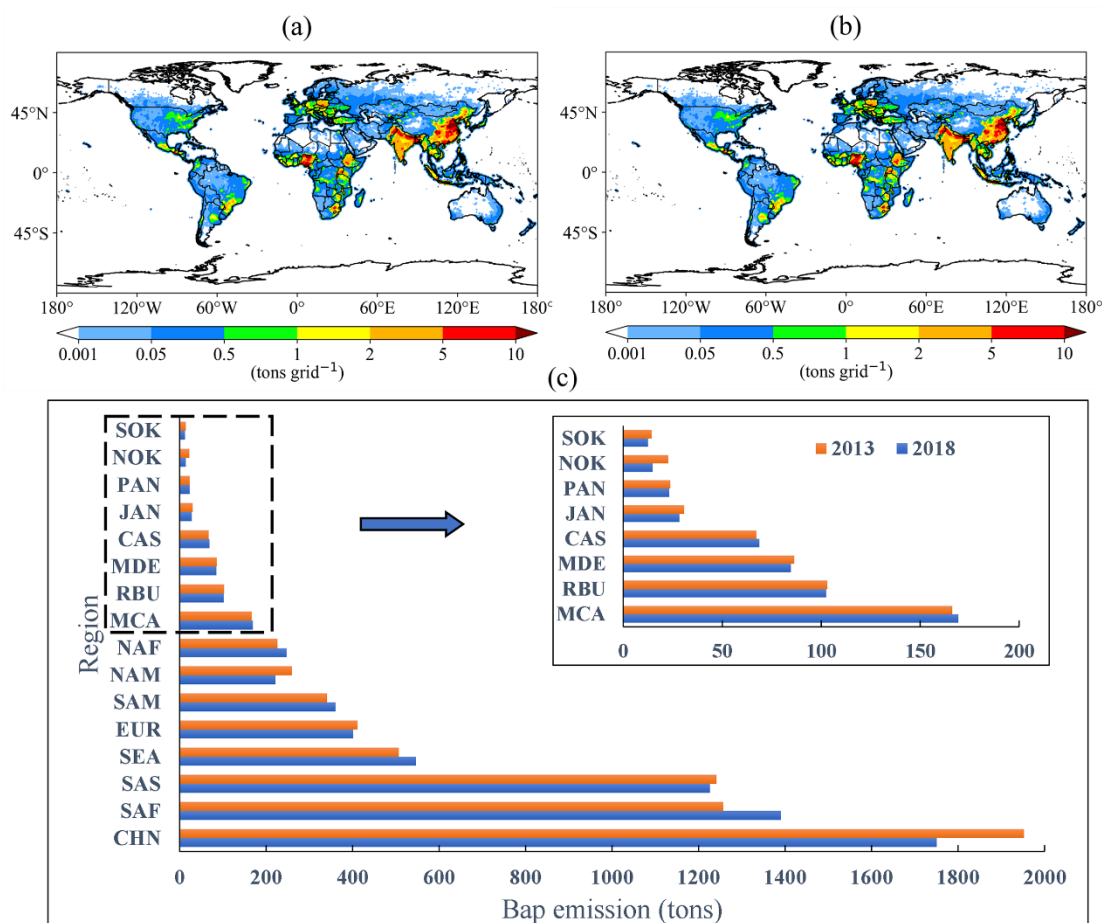
Figure 1. Spatial distributions of total emissions of BaP in (a) 2013 and (b) 2018 based on the EDGAR inventory. (c) BaP emissions for 16 regions (except oceans, Arctic, and Antarctic) in 2013 and 2018.

The global total emissions of BaP in 2013 and 2018 are shown in Fig. 1a and 1b, respectively. The annual emissions in different regions (Fig. S1) were also calculated (Fig. 1c). The global emissions of BaP were 7,166.9 t in 2013 and 7,109.5 t in 2018, respectively. Figure. S3 shows emissions and changes for different sectors in China, Africa, South Asia, Europe, North America, and Sorth America in 2013 and 2018, where resident, industry, and agriculture are the main sources of BaP. China is one of the largest BaP-emitting countries in the world. Its emissions were 1,952.2 t in 2013 and 1,750.2 t in 2018, respectively, accounting for about 27.2% and 24.6% of the world, which are generally consistent with the results of Shen et al. (2013) (20.3%). The residential sector is the largest emission source of BaP in China, accounting for 63.2% of the total emissions, followed by industrial sector (35.6%) in 2013. Africa and South Asia had the second and third-largest emissions, with residential combustion accounting for 87.3% and 84.0% of total emissions, respectively. This is related to the widespread use of biomass fuels for heating and cooking in developing countries (Shen et al., 2013). Emissions from China, Southern

275   Africa, and South Asia accounted for 62.1% and 61.4% of the world. China, Australia, South Asia,

276   Europe, North America, South Korea, Japan, and North Korea displayed a declining trend from 2013 to

277   2018. China experienced the largest decline (10.4%), due to the active emission control measures taken

278   under the "Air Pollution Prevention and Control Action Plan" implemented in 2013. The industrial sector

279   contributed the most to the decline of BaP emissions, followed by the residential combustion, which

280   decreased by 18.9% and 5.1% from 2013 to 2018, respectively, which are mainly related to the

281   strengthened industrial emission standards, upgraded industrial boilers, and the development of clean

282   fuels. The above results are generally consistent with the conclusions of Wang et al. (2021) in which

283   PAHs emissions decreased by 11.36% from 2013 to 2017, with the industrial and residential sectors

284   decreasing by 17.32% and 10.58%, respectively. The emissions increased in Africa (10.3%) and South

285   America (5.9%), mainly caused by the emission increase in residential (10.6%) and agricultural (9.5%)

286   sectors, respectively.

287   To understand the change in BaP concentrations, we conducted five experiments: the first and

288   second experiments simulated the BaP concentration using the emissions in 2013 and 2018 driven by the

289   corresponding meteorological fields. The third experiment used the emission in 2018 but kept the

290   meteorological conditions in 2013 to investigate the effects of meteorological condition changes on the

291   concentration of BaP. Studies neglecting the heterogeneous loss of BaP and using two different

292   heterogeneous schemes were also performed to explore the impacts of heterogeneous reactions on BaP

293   concentrations in the fourth and fifth experiments

294   **3.2 Observational data**

295   To evaluate the model performance, we collected the PAHs observation from several available

296   datasets and more than 50 published papers. The observational data are summarized as follows: (1)

297   European   Monitoring   and   Evaluation   Program   (EMEP,   available   from

298   https://projects.nilu.no/ccc/reports.html, last access: 15 December 2023): this includes annual and

299   monthly averages of BaP concentrations at 36 European sites in Spain, Finland, France, Germany,

300   Norway, Poland, and other countries in Europe; (2) National Air Pollution Surveillance network: (NAPS,

301   https://data-donnees.az.ec.gc.ca/data/air/monitor/: last access:30 January 2024): this includes daily

302   averages (autumn and winter) of BaP concentrations at Canadian stations; (3) Integrated Atmospheric

303   Deposition Network: (IADN, https://iadnviz.iu.edu/datasets/index.html, last access: 20 January 2023):

this includes monthly mean concentrations of BaP at 6 sites in the United States and Canada from 1990 to 2021; (4) Chinese Persistent Organic Pollutants (POPs) Soil and Air Monitoring Program Phase II (SAMP-II, Ma et al., 2018): this is carried out by the International Joint Research Center for Persistent Toxic Substances (IJRC-PTS), focusing on 11 urban centers in China (Beijing, Xi'an, Nanchang, Kunming, Lanzhou, Chengdu, Harbin, Dalian, Lhasa, Guangzhou, and Shihezi), 1 suburb and 3 background/rural areas. This observational data only covers the period from August 2008 to July 2010; (5) observational data collected from published papers (these sources are listed in supplementary material) (Wu et al., 2024).

PAHs measurements data are very sparse compared to conventional pollutants (e.g., $PM_{2.5}$). Since most of the data are not continuous in time, we selected data covering at least 10 days in years as close as possible to the simulation year (2013) and used the mean values for comparison. The comparison of the monthly variation was conducted only for sites in Europe where observations were continuous and available. The locations of the BaP observation sites are shown in Fig. S2. The site information is listed in Table S5 and Table S6.

4 Results

4.1 Global distribution of BaP and health risks
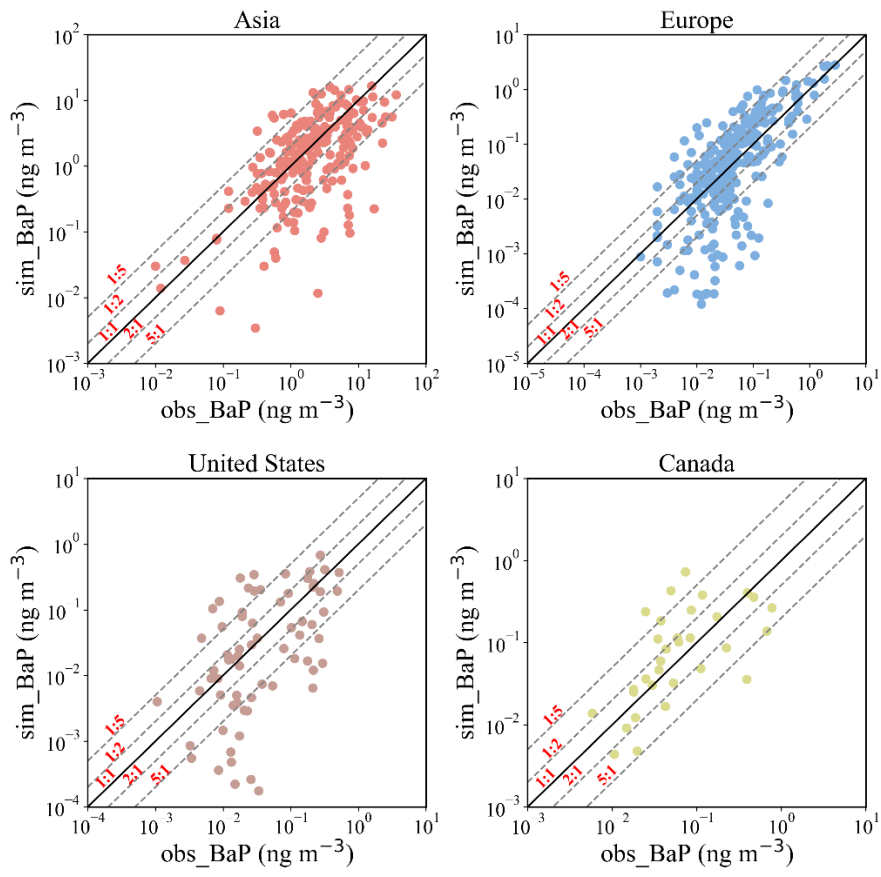
320
321 **Figure 2. Comparison of simulated (sim_BaP) and observed (obs_BaP) annual mean concentrations of BaP**
322 **in Asia (pink), Europe (blue), United States (brown), and Canada (green) in 2013. The solid black line shows**
323 **a ratio of 1 : 1 and the dashed gray lines show ratios of 5 : 1, 2 : 1, 1 : 2, and 1 : 5.**
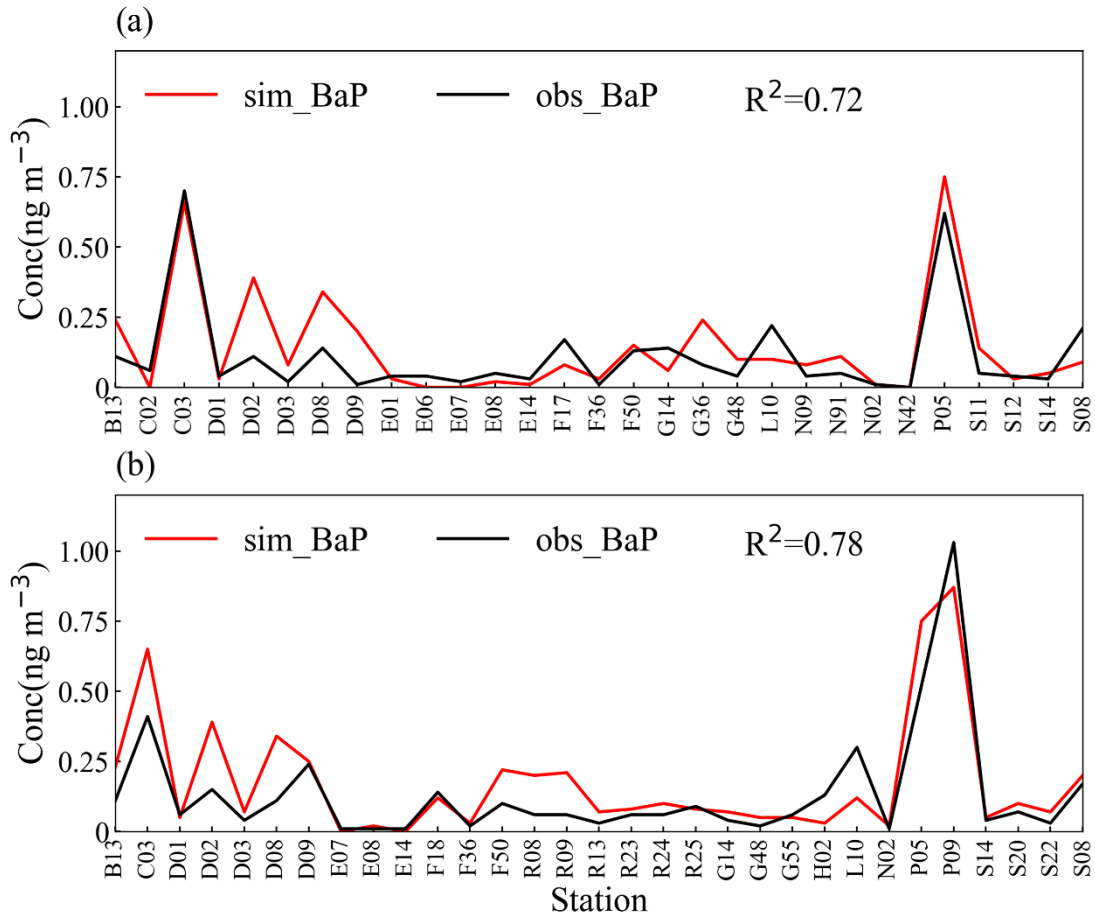
Figure 3. Comparison of the BaP annual mean simulated (red) concentrations with observed (black) values at European sites in (a) 2013 and (b) 2018.

To evaluate the performance of the IAP-AACM model, annual mean simulated concentrations in Asia, Europe, the United States, and Canada were compared with observations (Fig. 2). The results show that the model can reproduce nearly half of the observation samples within a factor of 2 and most observations within a factor of 5 at sites in Asia, Europe, the United States, and Canada. The number of sites where BaP was underestimated was greater than the number where it was overestimated due to the averaging effect of subgrid emissions. Considering that some of the comparisons are not in the same year, a certain discrepancy between the model and observation is expected. Further, a specific comparison was performed using the data from about 30 stations in Europe (Fig. 3a and b). High concentrations were mainly found in polluted areas of Central Europe, consistent with the simulation of Gusev et al. (2017), such as Poland (P05) and the Czech Republic (C03) with observed values of 0.70 and 0.62 ng m^{-3}, respectively, and simulated concentrations of 0.66 and 0.75 ng m^{-3} in 2013, The model successfully reproduced the observed concentrations and differences between sites.
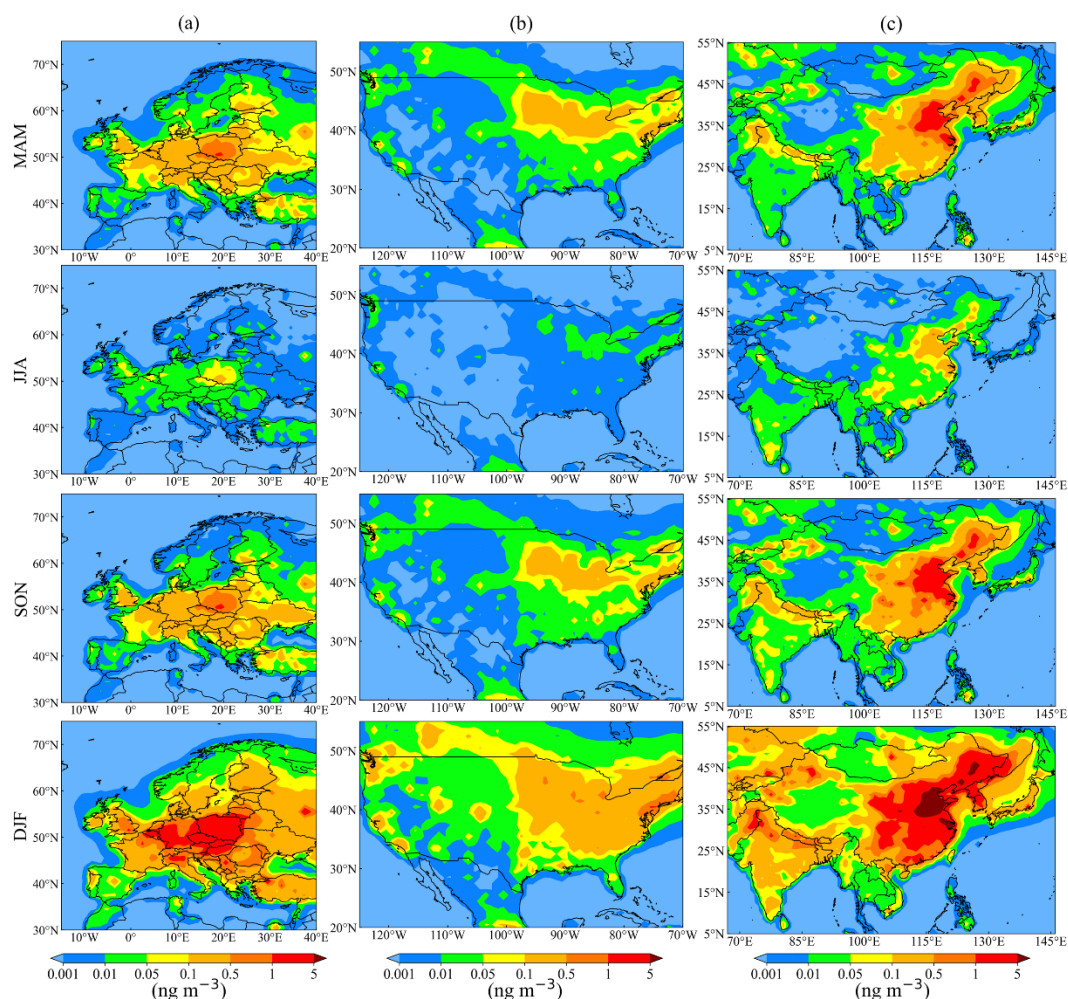
Figure 4. Spatial distributions of seasonal mean concentrations in (a) Europe, (b) the contiguous United States, and (c) East Asia in 2013.

Figure 4 shows the seasonal mean concentrations of BaP in Europe, the contiguous United States, and East Asia in four seasons: March–April–May (MAM, representing spring), June–July–August (JJA, representing summer), September–October–November (SON, representing autumn), and December–January–February (DJF, representing winter). Generally, BaP had the highest concentration in winter and lowest in summer. This is caused by the larger emission and poorer atmospheric diffusion conditions in winter than in summer. In the contiguous United States, the concentrations were lower than 1 ng m^{-3} in all four seasons, consistent with the simulation of Galarneau et al. (2014). In east China, large areas have a concentration of > 1 ng m^{-3} and even > 5 ng m^{-3} in BTH in winter. Europe shows a distribution of high values in central areas and low values in remote areas. In Central Europe (such as Poland and the Czech Republic), large areas have concentrations between 1–5 ng m^{-3} in winter. High concentrations were also reported by Bieser et al. (2012). The observation clearly shows higher concentrations at sites in Poland and the Czech Republic than at other sites in Europe (Fig. 5). The model successfully reproduces the

354   seasonal variation of BaP at sites in Europe. The simulation had a good agreement with observations at

355   C03 and P05 with correlation coefficient (R^2) of 0.91 and 0.91, and normalized mean bias (NMB) of -

356   0.04 and 0.14, respectively. The R^2 was higher than 0.8 at B13 and S08, and the NMB was 1.01 and -

357   0.55. In summary, IAP-AACM can reasonably simulate the spatial distribution and seasonal variation of

358   BaP.
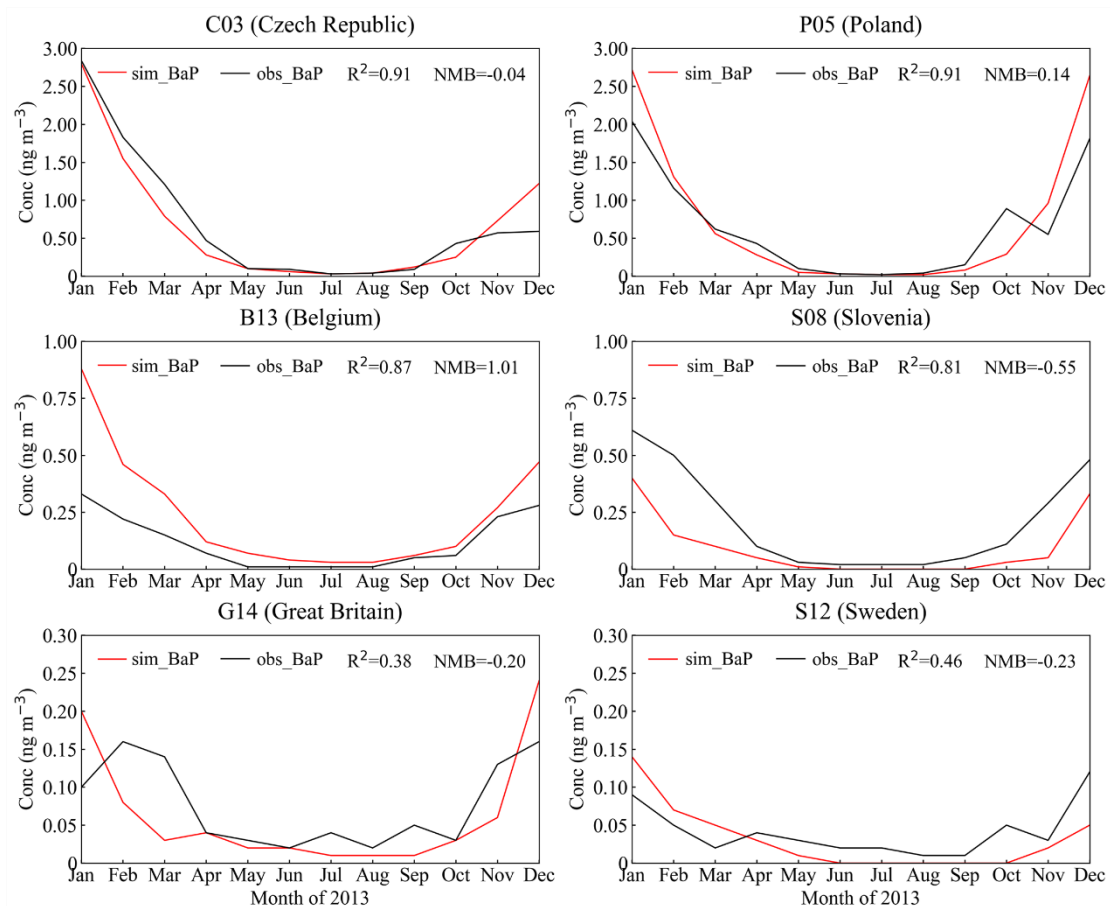
359

360   **Figure 5. Comparison of the BaP month mean simulated concentrations (red) with observed values (black)**

361   **at six stations in Europe in 2013.**

(a)   (b)

(c)   (d)

(e)   (f)
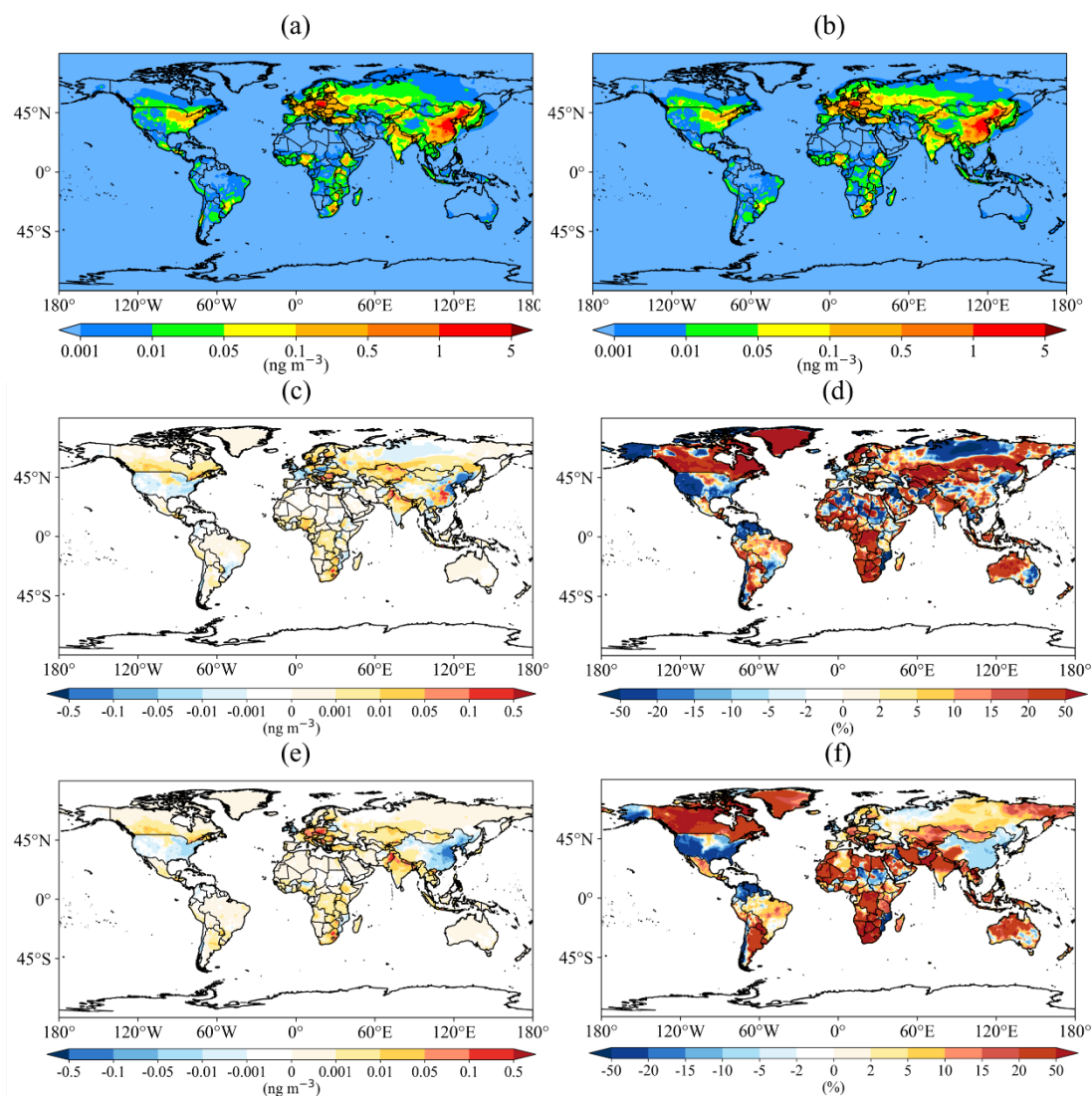
Figure 6. Spatial distributions of annual mean BaP concentrations based on the EDGAR in (a) 2013 and (b) 2018 . The (c/e) absolute and (d/f) relative concentration changes from 2013 to 2018 are shown considering (c, d) both emissions and meteorological conditions or (e, f) only emissions, respectively.

The spatial distribution of annual mean BaP concentrations based on the EDGAR inventory in 2013 and 2018 are shown in Fig. 6a and b. The spatial distribution of BaP concentrations in 2018 was similar to that in 2013. The spatial pattern was consistent with the emission distribution in the EDGAR inventory. High concentrations of BaP were found in northern and eastern China, and central Europe, even exceeding the European Union target value for BaP (1 ng m^{-3}), indicating an urgent need to control BaP and other PAHs. The absolute and relative concentration changes from 2013 to 2018 are shown in Fig. 6c and d. The most significant decreases were seen in Russia, the United States, eastern and northern China. By contrast, the concentration in India, Europe, Southeast Asia, and South Africa shows an increase, with the average annual concentration increasing by 19.4%, 1.2%, 11.2%, and 18.3%,

375 respectively. When only considering the impact of emission change (Fig. 6e and f), the decrease in the

376 eastern United States is larger and the increase in central Europe is larger. In particular, there is an obvious

377 decline (about 8.0%) across China, which demonstrates the effect of the emission reduction measures.

378 These results clearly show the large influence of meteorological changes. It is crucial to consider

379 meteorological factors when evaluating emission changes and reduction measures through monitoring

380 concentrations in the atmosphere.
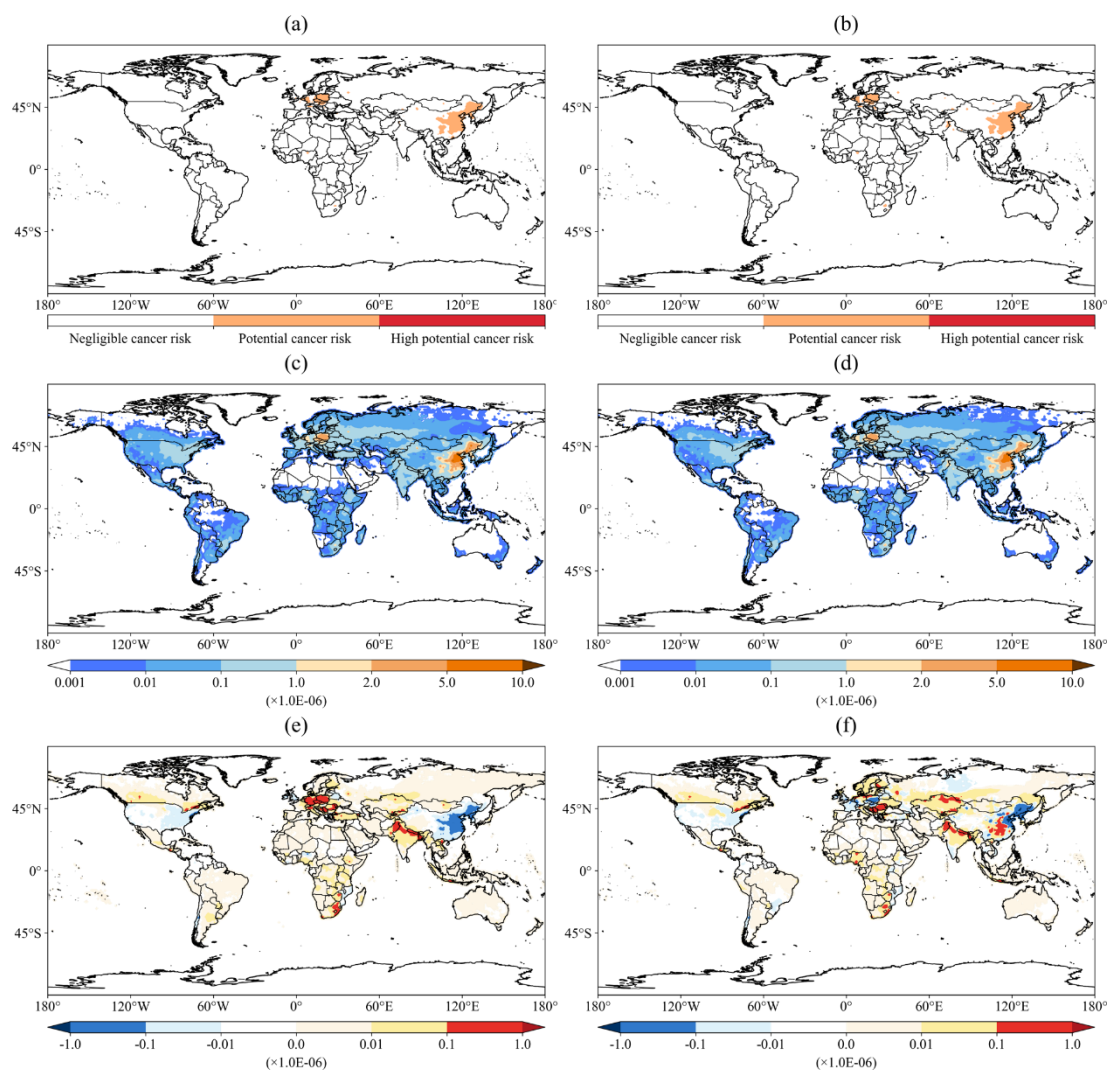
381
382 **Figure 7. The distribution of health risks grade in (a) 2013 and (b) 2018, the distribution of TILCR in (c)**
383 **2013 and (d) 2018, and the absolute from 2013 to 2018 when considering the change in (e) emissions only, (f)**
384 **both emissions and meteorological conditions.**

385 The global distribution of health risks grade and TILCR (the sum of ILCR values of the two

386 exposure routes after averaging the parameters of the different groups) in 2013 and 2018 are shown in

387 Fig. 7. It can be seen that most of the countries just face negligible cancer risk, and no regions facing

388 high potential cancer risk when evaluation is based on annual mean concentration. However, eastern

389   China and central Europe are in potential cancer risk, with the highest TILCR values of 1.54×10^{-5} (1.47

390    $\times 10^{-5}$) and $4.62 \times 10\text{-}6$ (4.23×10^{-6}) in 2013 (2018), respectively. It should be noted that in other

391   developing countries such as Africa, India, and Southeast Asia, TILCR values increased in 2018

392   compared to 2013, with the highest (mean) values increasing from 1.47×10^{-6} (4.15×10^{-8}) to 2.26×10^{-6}

393   (4.78×10^{-8}), from 1.41×10^{-6} (2.03×10^{-7}) to 1.73×10^{-6} (2.43×10^{-7}), and from 8.02×10^{-7} (6.07×10^{-8}) to

394   1.14×10^{-6} (6.75×10^{-8}), respectively. These countries will be likely to face potential even high potential

395   cancer risks, especially in winter. In addition, Lou et al. (2023) has indicated that health risks in South

396   Asia and Africa will increase in the future with the increase of residential fuels use along with the

397   population growth in these regions. It is clear that clean development is a necessary consideration for

398   developing countries to avoid the health risks posed by PAHs.

399   **4.2 Distribution of PAHs and their change in China**

400   Figure 8 shows the annual mean distribution of BaP in China in 2013. The concentrations ranged

401   from 0.02 to 6.14 ng m^{-3}. Overall, high concentrations were simulated in the North China Plain, East

402   China, and Northeast China, significantly higher than in Northwest and Southwest China, consistent with

403   previous studies (Ma et al., 2020; Yan et al., 2019). This can be largely attributed to the industrial and

404   residential coal combustion in these regions. Among the different provinces in China, there are 14

405   provinces with concentrations higher than the ambient air quality standards of China (1 ng m^{-3}, GB 3095–

406   2012: http://www.zhb.gov.cn/, last access: 6 April 2014). Shanghai had the highest concentration of 6.14

407   ng m^{-3}, followed by Tianjin (4.56 ng m^{-3}), Beijing (3.41 ng m^{-3}), and Shandong (3.10 ng m^{-3}). The

408   concentrations in the Northwest and Southwest regions were lower, with Tibet having the lowest

409   concentration of only 0.02 ng m^{-3}. This is due to lower levels of industrial activities and population

410   density in these regions compared to eastern regions. In addition, the high topography of northwest

411   regions has good air circulation and is conducive to the diffusion and dilution of atmospheric pollutants.

412   In 2013, Beijing had the highest BaP concentration in winter (14.03 ng m^{-3}), possibly due to the high

413   population density, high number of vehicles, and frequent industrial activities in Beijing. Moreover,

414   Beijing lies on the North China Plain, where the meteorological conditions make it easier for air

415   pollutants to stay and accumulate, resulting in a high concentration of BaP.

416
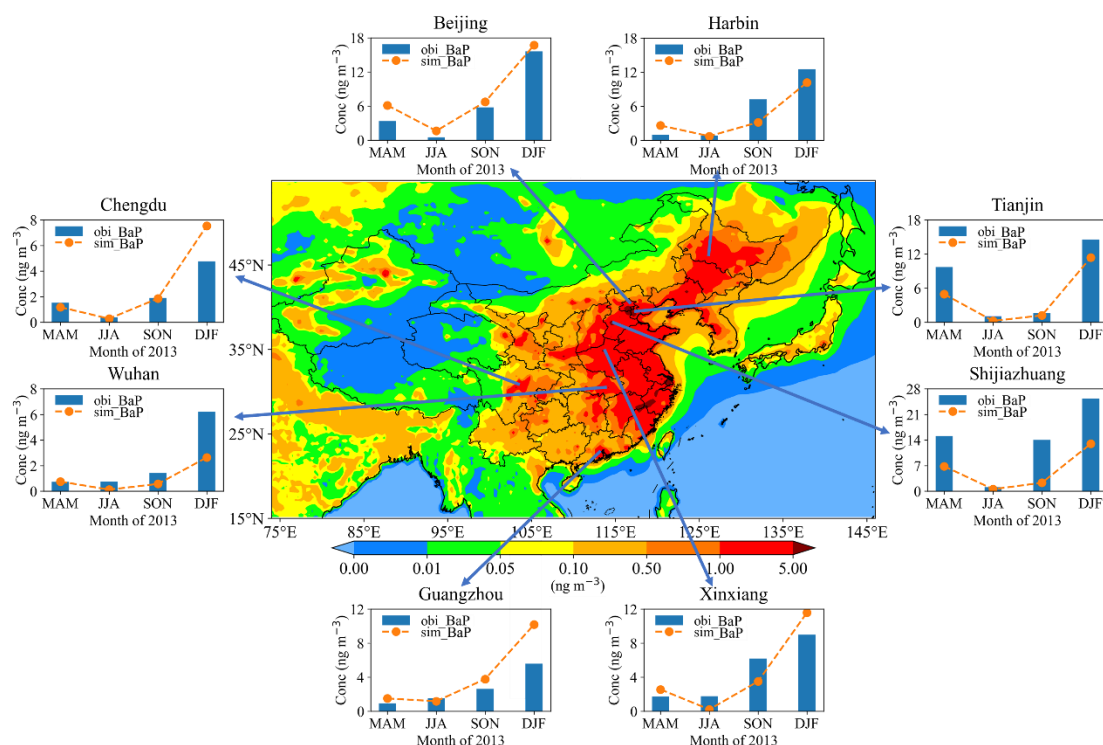
Figure 8. Spatial distributions of annual mean concentrations in China. Comparison of the BaP month mean simulated concentrations (orange) with observed values (blue) at eight cities in 2013.

To reveal the seasonal variation of BaP concentrations in key regions, we analyzed the concentration in eight major cities, i.e., Beijing, Tianjin, Shijiazhuang, Xinxiang, Wuhan, Chengdu, Guangzhou, and Harbin (seen in Fig. 8). It can be seen that the seasonal variations of BaP in these cities are similar, with the highest values in winter and the lowest in summer. The seasonal difference in northern cities was significantly greater than that in southern cities. In Beijing, Xinxiang, Tianjin, Harbin, and Shijiazhuang, the differences in concentration between winter and summer were as high as 15.06, 11.76, 11.14, 9.45, and 12.42 ng m^{-3}, respectively. This is caused by the fact that coal-fired heating is very common in northern China, which can significantly increase the PAH emissions in winter (Yan et al., 2019). In addition, the meteorological conditions also affect the seasonal variation of PAHs, as the lower temperature, less rainfall, and weaker solar radiation during the winter support the formation of a stable inversion layer, greatly limiting the diffusion of BaP in the air (Lin et al., 2015; Quan et al., 2014).

By comparing the simulated concentrations with the observed concentrations, we find that the model can capture the BaP concentrations and the seasonal pattern in different cities. For example, the observed and simulated concentrations show good consistency in the spring, summer, and autumn of Chengdu and in the summer, autumn, and winter of Beijing, with a deviation of only 0.04 to 1.1 ng m^{-3}. However, there were some deviations between the simulated and observed concentrations. The most obvious

435   underestimation is seen in Shijiazhuang. This is probably due to the underestimation of emissions and

436   the model resolution that may not fully resolve the pollution in cities with urban areas smaller than the

437   model grid. The model performance could be improved by using more precise emissions and increasing

438   grid resolution. Nonetheless, the model can capture the magnitude and seasonal variation in BaP

439   concentration well in China and in other countries around the world, and can therefore be used to evaluate

440   the health effects of BaP exposure.
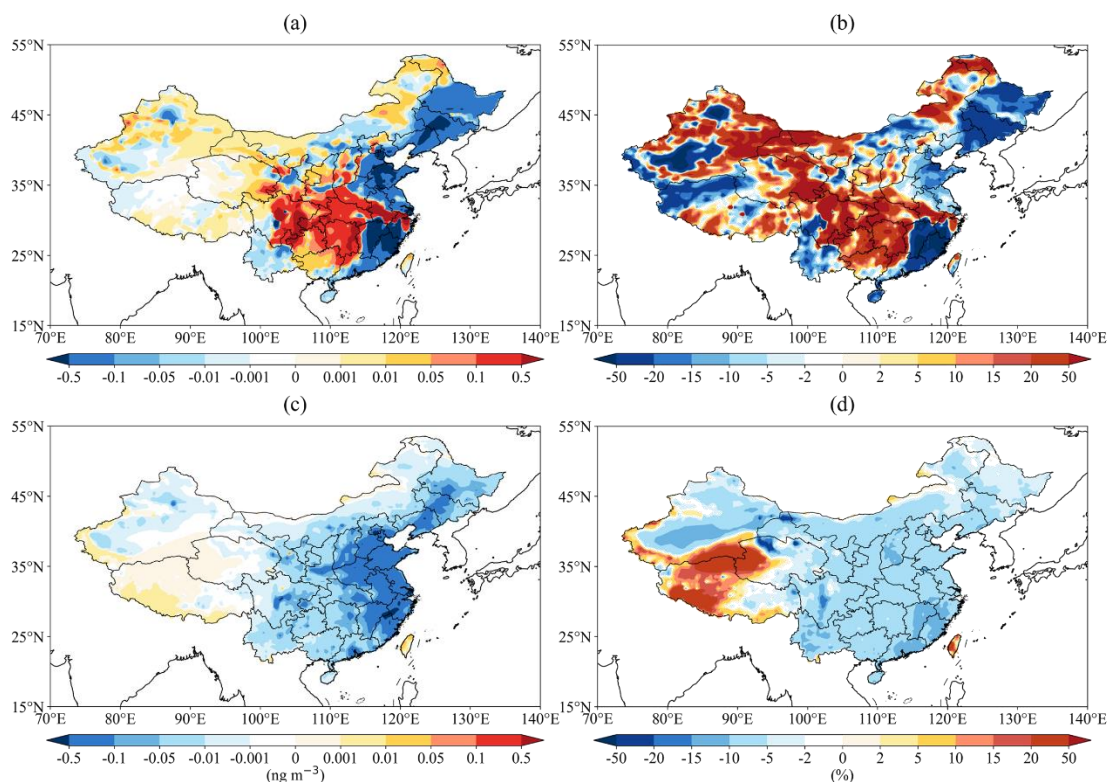
441
442   **Figure 9. The (a/c) absolute and (b/d) relative concentration changes from 2013 to 2018 in mean annual BaP**
443   **concentrations in China are shown considering (a, b) both emissions and meteorological conditions or (c, d)**
444   **only emissions, respectively.**

445   The changes from 2013 to 2018 are shown in Fig. 9. The trend and magnitude of changes differ

446   greatly across different regions. The largest decrease (> 20%) was seen in northeastern and southeastern

447   China, consistent with the other studies in Beijing (Lin et al., 2024), Shanghai (Yang et al., 2021),

448   Shenyang (Zhang et al., 2023), Tianjin (Zhang et al., 2022). The concentration also decreased in the

449   North China Plain, benefitting from the emission reduction policies such as the development of cleaner

450   energy sources and the control of industrial emissions. The concentration decrease was larger than the

451   emission reduction over these areas. By contrast, as shown in Fig. 9a, the concentration in the Sichuan

452   Basin showed an inverse trend although the emission decreased. This phenomenon demonstrates the

453   large impact of unfavorable meteorological conditions with decreasing temperatures and planetary

454   boundary layer height compared to 2013 (Ding et al., 2019). When only considering the emissions

455   changes, the concentration shows a decrease over most regions consistent with the emission change. It

456   should be noted that the decrease in BaP in the two experiments is significantly lower than that of $PM_{2.5}$.

457   As shown in Fig. 9b (Fig. 9d), the BaP concentration decreased by 9.1% and 6.7% (8.5% and 9.4%) in

458   the BTH and the YRD, respectively. Wang et al. (2019) showed that compared with 2013, the

459   concentration of $PM_{2.5}$ in the BTH, the YRD, and the PRD in 2017 decreased by 39.6%, 34.3%, and

460   27.7%, respectively. For cities in North and East China, the concentration still exceeds the national limit

461   value (1 ng m^{-3}) although the concentration of BaP decreased significantly in 2018. For example, the BaP

462   concentrations in Shanghai, Beijing, and Tianjin considering changes in both emissions and meteorology

463   were 5.32, 3.31, and 3.38 ng m^{-3}, respectively, and those with emission changes alone were 5.58, 3.11,

464   and 4.17 ng m^{-3}, indicating that the concentrations are mainly affected by the emission sources. The

465   results in the central and western cities differed greatly between the two experiments, especially in

466   Chongqing, Sichuan, and Guizhou, indicating that changes were mainly related to meteorological

467   conditions. Therefore, when formulating emission reduction policies, it is necessary to take into account

468   the effects of changes in meteorological conditions as well as emission sources.

469   **4.3 Health risks of PAHs in China**
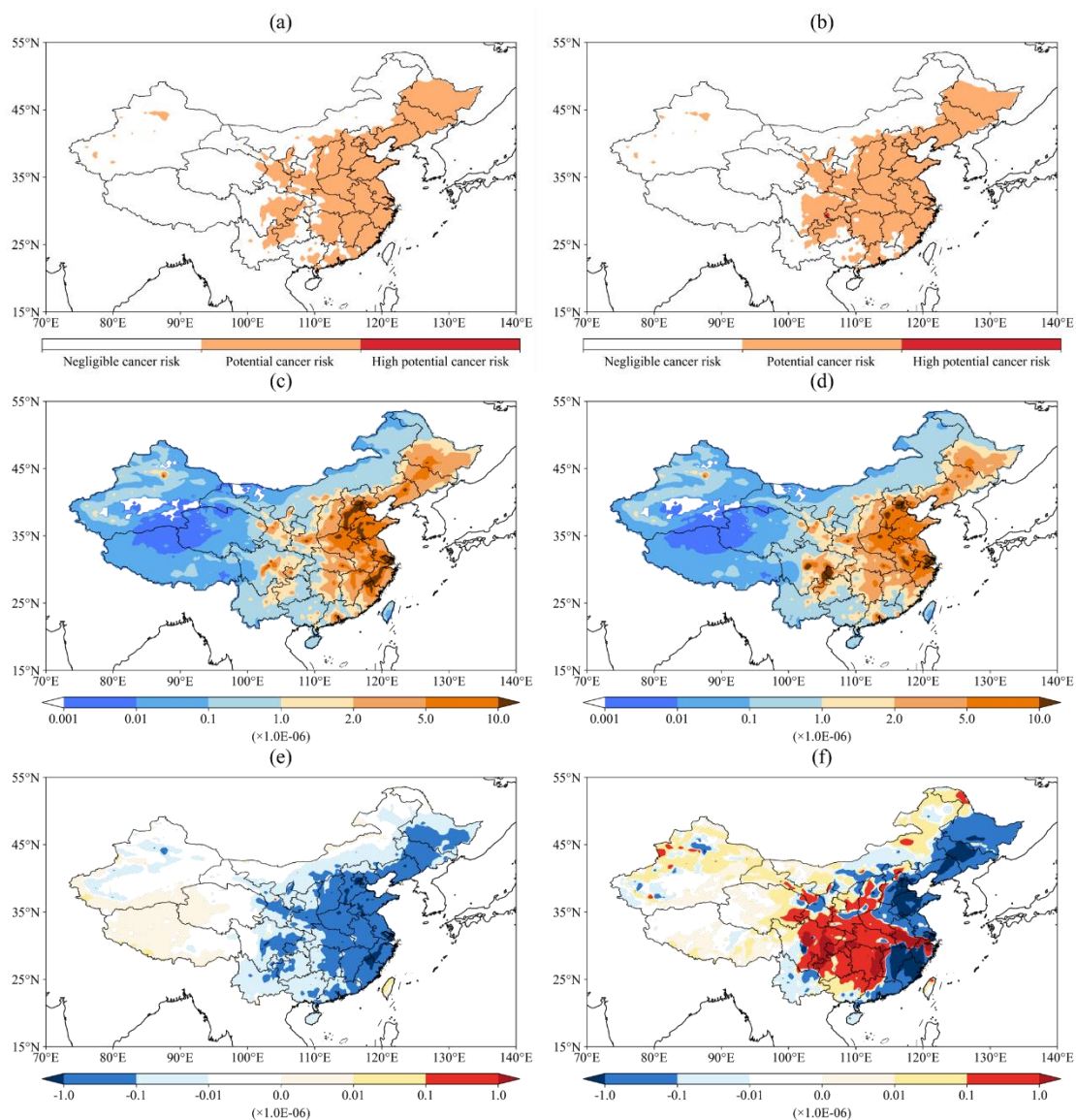
470
471 **Figure 10. The distribution of health risks grade in China in (a) 2013 and (b) 2018, the distribution of**
472 **TILCR in (c) 2013 and (d) 2018, and the TILCR changes from 2013 to 2018 when considering the change in**
473 **(c) emissions only, (f) both emissions and meteorological conditions.**

474   In this section, the health risks of BaP are assessed based on the simulation over the nested domain

475 (domain 2) covering China. As shown in Fig. 10a and b, the health risks in western China is negligible,

476 while there is a potential cancer risk in eastern China. Figure 9c and d show the TILCR values in 2013

477 and 2018, and Fig. 10e and f show the change from 2013 to 2018 when only emissions or both emissions

478 and meteorological conditions are considered. It can be seen that the spatial distribution of TILCR (Fig.

479 10c) is consistent with the spatial distribution of the BaP annual concentrations (Fig. 6), showing higher

480 risk in eastern regions than in the western regions (Han et al., 2020). The values of the TILCR in China

481 ranged from 3.0×10^{-9} to 3.5×10^{-5}, with an average value of 1.4×10^{-6}. Compared with 2013, the average

482 TILCR in 2018 decreased by 8.0×10^{-8}, which is mainly directly related to the decrease in concentration.

483 From the perspective of two exposure routes, $ILCR_{inh}$ and $ILCR_{der}$ values ranged from 2.8×10^{-10}–3.3×10^{-6}

484 and 2.7×10^{-9}–3.2×10^{-5}, with an average value of 1.3×10^{-2} and 1.3×10^{-6}, respectively. The values of

485 $ILCR_{der}$ were one order of magnitude higher than the $ILCR_{inh}$.
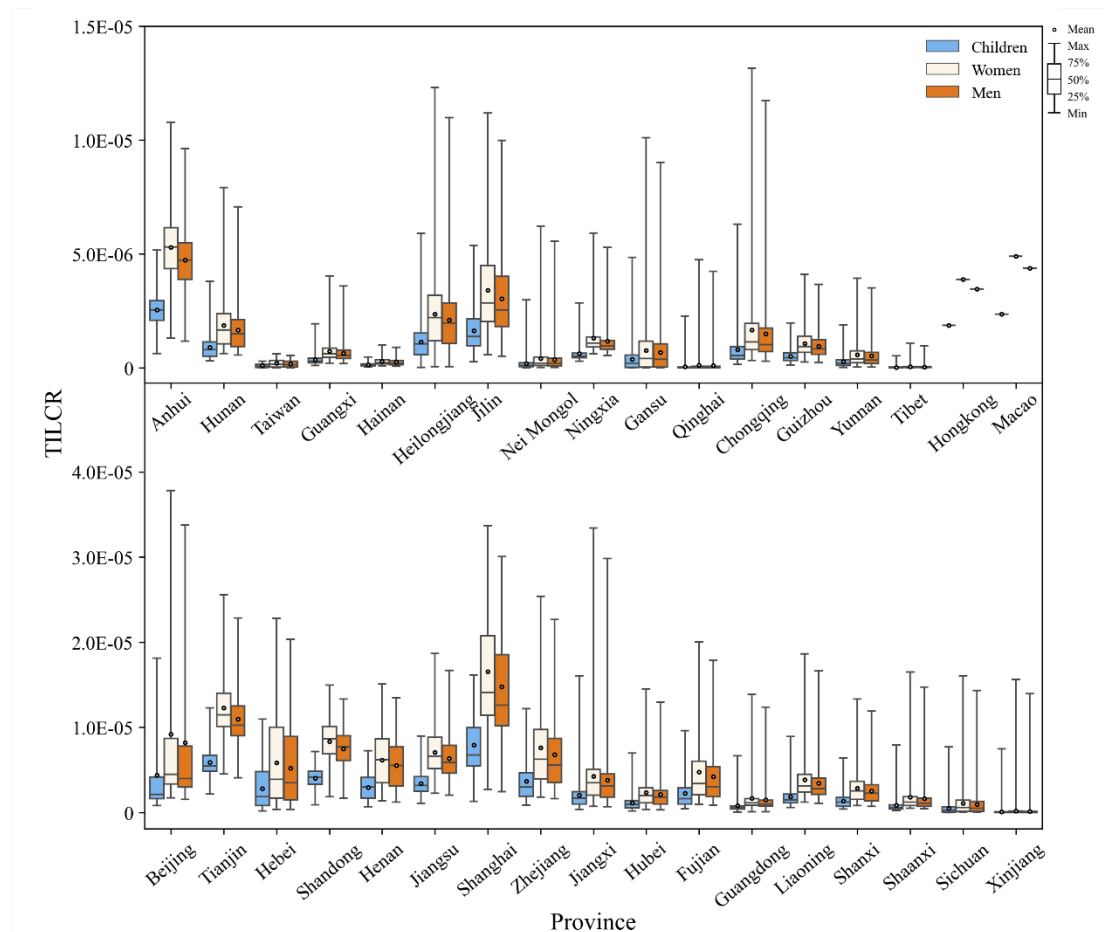
486
487 **Figure 11. The TILCR values for the three age groups (Children, Women, and Men) in different provinces**
488 **of China in 2013.**

489   The TILCR values of the three groups in 2013 and 2018 calculated using Eq. (14)-Eq. (18) are

490 shown in Fig. 11 and Fig. S4, respectively, which ranged from 1.55×10^{-9} to 3.78×10^{-5} (1.60×10^{-9} to

491 3.41×10^{-5}). The order of TILCR was women (1.46×10^{-6}) > men (1.31×10^{-6}) > children (7.03×10^{-7}), which

492 was similar to that of dermal contact exposure. Overall, 29.2% of TILCR were higher than 1.0×10^{-6}, and

493 1.2% of TILCR were higher than 1.0×10^{-5} in 2013. There was a slight decrease in TILCR values in 2018

494 due to the lower concentrations of BaP, with 27.9% and 0.7% of TILCR higher than 1.0×10^{-6} and 1.0×10^{-5}

495 respectively. There is no high cancer risk in China, but there are potential cancer risks in some areas,

496 which should be paid attention to.

497
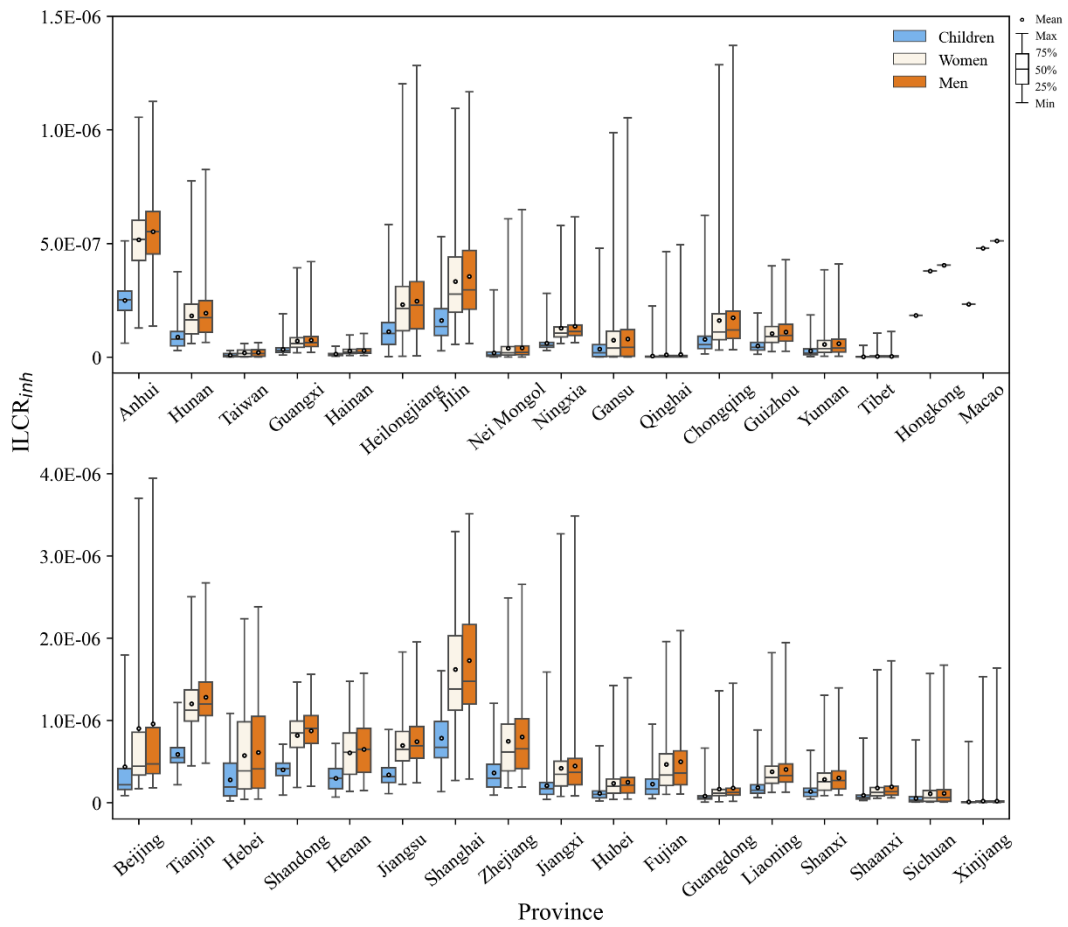
498 **Figure 12. The ILCR$_{inh}$ values for the three age groups (Children, Women, and Men) in different provinces**

499 **of China in 2013.**

Figure 13. The ILCR_der values for the three age groups (Children, Women, and Men) in different provinces of China in 2013.

The ILCR values of the three groups in China through inhalation and dermal exposure routes are shown in Fig. 12 and Fig. 13, and the ILCR in 2018 are shown in Fig. S5 and Fig. S6. For the inhalation pathway, the average $ILCR_{inh}$ was 1.22×10^{-7} ($< 1.0 \times 10^{-6}$). The order of $ILCR_{inh}$ was men (1.53×10^{-7}) > women (1.43×10^{-7}) > children (6.95×10^{-8}), and the risk for men was about twice that of children, but was lower in women than in men. This may be caused by the fact that the inhalation and metabolic rate of women are weaker than men (Bai et al., 2020). The highest average value was found in Shanghai, where the average $ILCR_{ing}$ for the three groups were 1.72×10^{-6}, 1.62×10^{-6}, and 7.84×10^{-7}, respectively. Han et al. (2020) found cases of excess cancer due to exposure to PAHs in large cities such as Shanghai. Only 1.6% of the three groups had $ILCR_{ing}$ higher than 1×10^{-6}, indicating that the health risks from inhalation exposure were low. A similar conclusion was mentioned in an earlier review (Yan et al., 2019).

For dermal contact exposure, the average $ILCR_{der}$ was 1.04×10^{-6} ($> 1.0 \times 10^{-6}$). Compared to the $ILCR_{inh}$, the health risk to adults was slightly higher than that to children, but women had higher risk

values than men. This may be caused by the fact that the body weight of women is weaker than men. The order of $ILCR_{der}$ was women (1.32×10^{-6}) > men (1.15×10^{-6}) > children (6.33×10^{-6}), which is similar to the results of previous studies (Bai et al., 2020). Among the three groups, 27.4% of the $ILCR_{der}$ values were higher than 1×10^{-6}, and 0.7% were higher than 1×10^{-5}. This shows that there is a greater potential carcinogenic risk through dermal contact exposure.

5 Discussion

It should be noted that model results have some uncertainties even though our model simulated the main features of PAHs concentrations reasonably well. Firstly, we simulated lower BaP concentrations when using the PKU inventory than when using the EDGAR inventory over most continental areas, except for Inner Mongolia, eastern Russia, and north China (Fig. S7). The difference can be as high as 0.5 ng m^{-3} over some areas in wintertime although the spatial and temporal distributions are consistent. The emission inventory remains to be constrained by more observations. Current observations are too sparse to conduct detailed evaluation in areas where long-term measurements are not available. Secondly, we tested the influence of heterogeneous reaction schemes on simulation. When heterogeneous reactions were not considered, the model significantly overestimated the concentration of BaP (Fig. S8), suggesting the importance of heterogeneous loss of BaP. Using the Langmuir-Hinshelwood mechanism, we simulated lower concentrations in most regions of the northern hemisphere, especially in winter (Fig. S9). However, the difference between the simulated results of the two mechanisms is significantly reduced in summer due to high temperature and high humidity. This is consistent with the results by Mu et al. (2018), i.e., low temperature and low humidity can significantly increase the lifetime of BaP. Comparison of model results using different schemes and model intercomparison would further help identify the uncertainties and improve model performance.

6 Conclusion

In this study, the PAHs modules were coupled into the IAP-AACM model to investigate the global and regional distribution of PAHs. The model has the state-of-the-art heterogeneous mechanism and allows us to consistently examine the multi-scale distribution of PAHs. Comparison with observations shows that the model can reproduce the different concentrations of BaP at the stations in Asia, Europe,

the United States, and Canada. The model can capture the seasonal variation of BaP, with lower concentrations in summer and higher concentrations in winter over the continents in the northern hemisphere. The global distributions of BaP in 2013 and 2018 were very similar, with high concentrations concentrated in eastern China and central Europe, even exceeding EU limits (1 ng m^{-3}). Compared with 2013, BaP concentration in 2018 showed a decrease in the United States, Poland, France, Czech, and some regions in China. By contrast, the concentrations increased by >10% in India and South Africa. Populations in these regions are facing increased health risks posed by PAHs.

In China, the decline in BTH (8.5%) and YRD (9.4%) benefitted from "the Action Plan". However, the decline was significantly less than that of conventional pollutants, such as $PM_{2.5}$. Changes in meteorological conditions had a significant influence on changes in BaP concentration, which increased in the Sichuan Basin and central China even though the emissions over these areas decreased due to the control measures. There was a slight decrease in total ILCR (TILCR) values in 2018 compared to 2013. For the different exposure routes, the dermal contact was an order of magnitude higher than the inhalation route. The TILCR for adults was greater than that for children. 29.2% of TILCR were higher than 1.0×10^{-6}, indicating that there are still potential cancer risks in China. More attention must be paid to the non-traditional pollutant pollutants and strict but different control measures are necessary to reduce PAHs' concentration and health risks. Especially in the fall and winter seasons, the concentration of BaP and the associated health risk is significantly higher than in other seasons. Management efforts on key sectors (e.g., industrial and residential sources) should be further strengthened. In heavily polluted cities, using clean energy to replace coal combustion, adjusting the energy structure of factory production, and developing innovative technologies with lower and even no emissions would be helpful to reduce PAHs pollution.

In summary, our study developed an effective tool for simulating the global and regional concentrations of BaP and other PAHs and quantified the health risks in China from 2013 to 2018. Model analysis indicated that emission inventories and heterogeneous reactions can significantly affect the simulated BaP concentrations. Accurate emissions and reasonable representation of heterogeneous reactions would greatly reduce the gap between model results and observation. However, the current observations are insufficient to fully evaluate and constrain the model. Especially, long-term observations are needed in Asia, India, and Africa. These regions are still facing significant health risks. In addition,

571 monitoring in the background and remote regions (such as the Arctic) is necessary to quantify the long-

572 range transport of PAHs.

573

574 *Code and data availability.* The source code and their introduction of IAP-AACM can be found online

575 via Zenodo (https://doi.org/10.5281/zenodo.12214119). The simulated data can be found via Zenodo

576 (https://doi.org/10.5281/zenodo.11595165). All the observational data are provided in the supplement

577 and can be found via Zenodo (https://doi.org/10.5281/zenodo.11595165).

578

579 *Author contributions.* ZcW developed the model, prepared the input data, performed the simulations and

580 analysis, and wrote the paper with suggestions from all co-authors. XC supported the coding and

581 conceived the idea of the paper. XC and ZfW revised the paper and provided scientific guidance through

582 all research advances. JL, ZW, LW, HC, YL, MQ, XT, and QW modified the manuscript. WW supported

583 the emission data. YW, ZZ, and ZJ supported the data analysis. All listed authors have read and approved

584 the final manuscript.

585

586 *Competing interests.* The authors declare that they have no conflict of interest.

587

590

591 *Acknowledgements.* We are particularly grateful to Prof. Oliver Wild at Lancaster University for his help

592 with improving the paper. We thank Prof. Alexey Gusev at EMEP for providing MSC-E results as a good

593 reference to test our model performance. We also thank the National Key Scientific and Technological

594 Infrastructure project "Earth System Science Numerical Simulator Facility" (EarthLab). We also thank

595 the editors and reviewers for providing constructive comments and suggestions to help us improve the

596 manuscript.

597

598 *Financial support.* This research has been supported by the National Key R&D Program of China (Grant

599 NO.2020YFA0607801), the National Natural Science Foundation of China (Grant NO. 42377105) and

600   the National Key Scientific and Technological Infrastructure project "Earth System Science Numerical

601   Simulator Facility".

602   **References**

603   Aulinger, A., Matthias, V.,Quante, M.: CMAQ simulations of the benzo(a)pyrene distribution over

604   Europe for 2000 and 2001, Atmospheric Environment, 43, 4078-4086,

605   https://doi.org/10.1016/j.atmosenv.2009.04.058, 2009.

606   Aulinger, A., Quante, M.,Matthias, V.: Introducing a Partitioning Mechanism for PAHs into the

607   Community Multiscale Air Quality Modeling System and Its Application to Simulating the

608   Transport of Benzo(a)pyrene over Europe, Journal of Applied Meteorology and Climatology,

609   46, 1718-1730, https://doi.org/10.1175/2007jamc1395.1, 2007.

610   Baek, S. O., Field, R. A., Goldstone, M. E., Kirk, P. W., Lester, J. N.,Perry, R.: A review of atmospheric

611   polycyclic aromatic-hydrocarbons-sources,fate and behavior, Water Air and Soil Pollution, 60,

612   279-300, https://doi.org/10.1007/bf00282628, 1991.

613   Bai, L., Chen, W. Y., He, Z. J., Sun, S. Y.,Qin, J.: Pollution characteristics, sources and health risk

614   assessment of polycyclic aromatic hydrocarbons in PM2.5 in an office building   in northern

615   areas, China, Sustainable Cities and Society, 53, 10, https://doi.org/10.1016/j.scs.2019.101891,

616   2020.

617   Bieser, J., Aulinger, A., Matthias, V.,Quante, M.: Impact of Emission Reductions between 1980 and 2020

618   on Atmospheric Benzo (a) pyrene Concentrations over Europe, Water Air and Soil Pollution,

619   223, 1393-1414, https://doi.org/10.1007/s11270-011-0953-z, 2012.

620   Byun, D.,Schere, K. L.: Review of the governing equations, computational algorithms, and other

621   components of the models-3 Community Multiscale Air Quality (CMAQ) modeling system,

622   Applied Mechanics Reviews, 59, 51-77, https://doi.org/10.1115/1.2128636, 2006.

623   Byun, D. W.,Dennis, R.: DESIGN ARTIFACTS IN EULERIAN AIR-QUALITY MODELS -

624   EVALUATION OF THE EFFECTS OF LAYER THICKNESS AND VERTICAL PROFILE

625   CORRECTION ON SURFACE OZONE CONCENTRATIONS, Atmospheric Environment, 29,

626   105-126, https://doi.org/10.1016/1352-2310(94)00225-a, 1995.

627   Cao, X. H., Huo, S. L., Zhang, H. X., Zheng, J. Q., He, Z. S., Ma, C. Z.,Song, S.: Source emissions and

628   climate change impacts on the multimedia transport and fate of persistent organic pollutants,

629   Chaohu watershed, eastern China, Journal of Environmental Sciences, 109, 15-25,

630   https://doi.org/10.1016/j.jes.2021.02.028, 2021.

631 Chen, H. S., Wang, Z. F., Li, J., Tang, X., Ge, B. Z., Wu, X. L., Wild, O.,Carmichael, G. R.: GNAQPMS-

632 Hg v1.0, a global nested atmospheric mercury transport model: model description, evaluation

633 and application to trans-boundary transport of Chinese anthropogenic emissions, Geoscientific

634 Model Development, 8, 2857-2876, https://doi.org/10.5194/gmd-8-2857-2015, 2015.

635 Chen, S. C.,Liao, C. M.: Health risk assessment on human exposed to environmental polycyclic aromatic

636 hydrocarbons pollution sources, Science of the Total Environment, 366, 112-123,

637 https://doi.org/10.1016/j.scitotenv.2005.08.047, 2006.

638 Chen, X. S., Wang, Z. F., Li, J.,Yu, F. Q.: Development of a Regional Chemical Transport Model with

639 Size-Resolved Aerosol Microphysics and Its Application on Aerosol Number Concentration

640 Simulation over China, Sola, 10, 83-87, https://doi.org/10.2151/sola.2014-017, 2014.

641 Chen, X. S., Yu, F. Q., Yang, W. Y., Sun, Y. L., Chen, H. S., Du, W., Zhao, J., Wei, Y., Wei, L. F., Du, H.

642 Y., Wang, Z., Wu, Q. Z., Li, J., An, J. L.,Wang, Z. F.: Global-regional nested simulation of

643 particle number concentration by combing microphysical processes with an evolving organic

644 aerosol module, Atmospheric Chemistry and Physics, 21, 9343-9366,

645 https://doi.org/10.5194/acp-21-9343-2021, 2021.

646 Crippa, M., Solazzo, E., Huang, G. L., Guizzardi, D., Koffi, E., Muntean, M., Schieberle, C., Friedrich,

647 R.,Janssens-Maenhout, G.: High resolution temporal profiles in the Emissions Database for

648 Global Atmospheric Research, Scientific Data, 7, 17, https://doi.org/10.1038/s41597-020-0462-

649 2, 2020.

650 Dachs, J.,Eisenreich, S. J.: Adsorption onto aerosol soot carbon dominates gas-particle partitioning of

651 polycyclic aromatic hydrocarbons, Environmental Science & Technology, 34, 3690-3697,

652 https://doi.org/10.1021/es991201+, 2000.

653 Ding, D., Xing, J., Wang, S.X., Liu, K.Y., Hao, J.M.: Estimated Contributions of Emissions Controls,

654 Meteorological Factors, Population Growth, and Changes in Baseline Mortality to Reductions

655 in Ambient PM2.5 and PM2.5-Related Mortality in China, 2013-2017. Environmental Health

656 Perspectives, 127, 12, https://doi.org/10.1289/ehp4157, 2019.

657 Dong, Z. S., Kong, Z. H., Dong, Z., Shang, L. Q., Zhang, R. Q., Xu, R. X.,Li, X.: Air pollution prevention

658 in central China: Effects on particulate-bound PAHs from 2010 to 2018, Journal of

659 Environmental Management, 344, 11, https://doi.org/10.1016/j.jenvman.2023.118555, 2023.

Du, H. Y., Li, J., Chen, X. S., Wang, Z. F., Sun, Y. L., Fu, P. Q., Li, J. J., Gao, J.,Wei, Y.: Modeling of aerosol property evolution during winter haze episodes over a megacity cluster in northern China: roles of regional transport and heterogeneous reactions of SO_2, Atmospheric Chemistry and Physics, 19, 9351-9370, https://doi.org/10.5194/acp-19-9351-2019, 2019.

Efstathiou, C. I., Matejovičová, J., Bieser, J.,Lammel, G.: Evaluation of gas-particle partitioning in a regional air quality model for organic pollutants, Atmospheric Chemistry and Physics, 16, 15327-15345, https://doi.org/10.5194/acp-16-15327-2016, 2016.

Feng, Y. Y., Ning, M., Lei, Y., Sun, Y. M., Liu, W.,Wang, J. N.: Defending blue sky in China: Effectiveness of the "Air Pollution Prevention and Control Action Plan" on air quality improvements from 2013 to 2017, Journal of Environmental Management, 252, 13, https://doi.org/10.1016/j.jenvman.2019.109603, 2019.

Finlayson-Pitts, B. J.,Pitts, J. N. Chemistry of the Upper and Lower Atmosphere: Theory, Experiments, and Applications. 2000.

Friedman, C. L., Pierce, J. R.,Selin, N. E.: Assessing the Influence of Secondary Organic versus Primary Carbonaceous Aerosols on Long-Range Atmospheric Polycyclic Aromatic Hydrocarbon Transport, Environmental Science & Technology, 48, 3293-3302, https://doi.org/10.1021/es405219r, 2014.

Friedman, C. L.,Selin, N. E.: Long-Range Atmospheric Transport of Polycyclic Aromatic Hydrocarbons: A Global 3-D Model Analysis Including Evaluation of Arctic Sources, Environmental Science & Technology, 46, 9501-9510, https://doi.org/10.1021/es301904d, 2012.

Galarneau, E., Makar, P. A., Zheng, Q., Narayan, J., Zhang, J., Moran, M. D., Bari, M. A., Pathela, S., Chen, A.,Chlumsky, R.: PAH concentrations simulated with the AURAMS-PAH chemical transport model over Canada and the USA, Atmospheric Chemistry and Physics, 14, 4065-4077, https://doi.org/10.5194/acp-14-4065-2014, 2014.

Gusev, A., Ilyin, I., Rozovskaya, O., Shatalov, V., Travnikov, O., Strijkina I. Assessment of transboundary pollution by toxic substances: Heavy metals and POPs, Meteorological Synthesizing Centre - East, Russia, 74 pp., 2019.

Han, F. L., Guo, H., Hu, J. L., Zhang, J., Ying, Q.,Zhang, H. L.: Sources and health risks of ambient

689   polycyclic aromatic hydrocarbons in China, Science of the Total Environment, 698, 13,

690   https://doi.org/10.1016/j.scitotenv.2019.134229, 2020.

691 Hansen, K. M., Christensen, J. H., Brandt, J., Frohn, L. M.,Geels, C.: Modelling atmospheric transport

692   of α-hexachlorocyclohexane in the Northern Hemispherewith a 3-D dynamical model: DEHM-

693   POP, Atmos. Chem. Phys., 4, 1125-1137, https://doi.org/10.5194/acp-4-1125-2004, 2004.

694 Haritash, A. K.,Kaushik, C. P.: Biodegradation aspects of Polycyclic Aromatic Hydrocarbons (PAHs): A

695   review, Journal of Hazardous Materials, 169, 1-15,

696   https://doi.org/10.1016/j.jhazmat.2009.03.137, 2009.

697 Harner, T.,Bidleman, T. F.: Octanol-air partition coefficient for describing particle/gas partitioning of

698   aromatic compounds in urban air, Environmental Science & Technology, 32, 1494-1502,

699   https://doi.org/10.1021/es970890r, 1998.

700 Inomata, Y., Kajino, M., Sato, K., Ohara, T., Kurokawa, J., Ueda, H., Tang, N., Hayakawa, K., Ohizumi,

701   T.,Akimoto, H.: Source contribution analysis of surface particulate polycyclic aromatic

702   hydrocarbon concentrations in northeastern Asia by source-receptor relationships,

703   Environmental Pollution, 182, 324-334, https://doi.org/10.1016/j.envpol.2013.07.020, 2013.

704 Inomata, Y., Kajino, M., Sato, K., Ohara, T., Kurokawa, J. I., Ueda, H., Tang, N., Hayakawa, K., Ohizumi,

705   T.,Akimoto, H.: Emission and Atmospheric Transport of Particulate PAHs in Northeast Asia,

706   Environmental Science & Technology, 46, 4941-4949, https://doi.org/10.1021/es300391w,

707   2012.

708 Jonker, M. T. O.,Koelmans, A. A.: Sorption of polycyclic aromatic hydrocarbons and polychlorinated

709   biphenyls to soot and soot-like materials in the aqueous environment mechanistic considerations,

710   Environmental Science & Technology, 36, 3725-3734, https://doi.org/10.1021/es020019x, 2002.

711 Jury, W. A., Spencer, W. F.,Farmer, W. J.: Behavior Assessment Model for Trace Organics in Soil: I.

712   Model Description, Journal of Environmental Quality, 12, 558-564,

713   https://doi.org/10.2134/jeq1983.00472425001200040025x, 1983.

714 Kahan, T. F., Kwamena, N. O. A.,Donaldson, D. J.: Heterogeneous ozonation kinetics of polycyclic

715   aromatic hydrocarbons on organic films, Atmospheric Environment, 40, 3448-3459,

716   https://doi.org/10.1016/j.atmosenv.2006.02.004, 2006.

717 Karickhoff, S. W.: Semi-empirical estimation of sorption of hydrophobic pollutants on natural sediments

and soils, Chemosphere, 10, 833-846, https://doi.org/10.1016/0045-6535(81)90083-7, 1981.

Keyte, I. J., Harrison, R. M.,Lammel, G.: Chemical reactivity and long-range transport potential of polycyclic aromatic hydrocarbons - a review, Chemical Society Reviews, 42, 9333-9391, https://doi.org/10.1039/c3cs60147a, 2013.

Klöpffer, W., Wagner, B.,Scheringer, M.: Atmospheric degradation of organic substances data for persistence and long-range transport potential, Environmental Science and Pollution Research - International, 14, 143-144, https://doi.org/10.1065/espr2007.04.408, 2007.

Kwamena, N. O. A., Clarke, J. P., Kahan, T. F., Diamond, M. L.,Donaldson, D. J.: Assessing the importance of heterogeneous reactions of polycyclic aromatic hydrocarbons in the urban atmosphere using the Multimedia Urban Model, Atmospheric Environment, 41, 37-50, https://doi.org/10.1016/j.atmosenv.2006.08.016, 2007.

Lammel, G., Dvorská, A., Klánová, J., Kohoutek, J., Kukacka, P., Prokes, R.,Sehili, A. M.: Long-range Atmospheric Transport of Polycyclic Aromatic Hydrocarbons is Worldwide Problem - Results from Measurements at Remote Sites and Modelling, Acta Chimica Slovenica, 62, 729-735, 2015.

Lammel, G.,Sehili, A. M.: Global fate and distribution of polycyclic aromatic hydrocarbons emitted from Europe and Russia, Atmospheric Environment, 41, 8301-8315, https://doi.org/10.1016/j.atmosenv.2007.06.050, 2007.

Lammel, G., Sehili, A. M., Bond, T. C., Feichter, J.,Grassl, H.: Gas/particle partitioning and global distribution of polycyclic aromatic hydrocarbons--a modelling approach, Chemosphere, 76, 98-106, https://doi.org/10.1016/j.chemosphere.2009.02.017, 2009.

Li, J., Wang, Z. F., Zhuang, G., Luo, G., Sun, Y.,Wang, Q.: Mixing of Asian mineral dust with anthropogenic pollutants over East Asia: a model case study of a super-duststorm in March 2010, Atmospheric Chemistry and Physics, 12, 7591-7607, https://doi.org/10.5194/acp-12-7591-2012, 2012.

Li, R. F., Zhang, J.,Krebs, P.: Global trade drives transboundary transfer of the health impacts of polycyclic aromatic hydrocarbon emissions, Communications Earth & Environment, 3, 13, https://doi.org/10.1038/s43247-022-00500-y, 2022.

Li, Z., Mulholland, J. A., Romanoff, L. C., Pittman, E. N., Trinidad, D. A., Lewin, M. D.,Sjödin, A.: Assessment of non-occupational exposure to polycyclic aromatic hydrocarbons through

personal air sampling and urinary biomonitoring, Journal of Environmental Monitoring, 12, 1110-1118, https://doi.org/10.1039/c000689k, 2010.

Lin, Y., Ma, Y. Q., Qiu, X. H., Li, R., Fang, Y. H., Wang, J. X., Zhu, Y. F.,Hu, D.: Sources, transformation, and health implications of PAHs and their nitrated, hydroxylated, and oxygenated derivatives in PM2.5 in Beijing, Journal of Geophysical Research-Atmospheres, 120, 7219-7228, https://doi.org/10.1002/2015jd023628, 2015.

Lin, Y., Shi, X. D., Qiu, X. H., Jiang, X., Liu, J. M., Zhong, P. W., Ge, Y. H., Tseng, C.-H., Zhang, J. F., Zhu, T., Araujo, J. A., Zhu, Y. F.: Reduction in polycyclic aromatic hydrocarbon exposure in Beijing following China's clean air actions. Science Bulletin, https://doi.org/10.1016/j.scib.2024.08.015, 2024.

Liu, S. J., Lu, Y. L., Wang, T. Y., Xie, S. W., Jones, K. C.,Sweetman, A. J.: Using gridded multimedia model to simulate spatial fate of Benzo α pyrene on regional scale, Environment International, 63, 53-63, https://doi.org/10.1016/j.envint.2013.10.015, 2014.

Lou, S. J., Shrivastava, M., Ding, A. J., Easter, R. C., Fast, J. D., Rasch, P. J., Shen, H. Z., Simonich, S. M., Smith, S. J., Tao, S.,Zelenyuk, A.: Shift in Peaks of PAH-Associated Health Risks From East Asia to South Asia and Africa in the Future, Earths Future, 11, 15, https://doi.org/10.1029/2022ef003185, 2023.

Ma, W. L., Liu, L. Y., Jia, H. L., Yang, M.,Li, Y. F.: PAHs in Chinese atmosphere Part I: Concentration, source and temperature dependence, Atmospheric Environment, 173, 330-337, https://doi.org/10.1016/j.atmosenv.2017.11.029, 2018.

Ma, W. L., Zhu, F. J., Liu, L. Y., Jia, H. L., Yang, M.,Li, Y. F.: PAHs in Chinese atmosphere Part II: Health risk assessment, Ecotoxicology and Environmental Safety, 200, 9, https://doi.org/10.1016/j.ecoenv.2020.110774, 2020.

Mu, Q., Shiraiwa, M., Octaviani, M., Ma, N., Ding, A. J., Su, H., Lammel, G., Pöschl, U.,Cheng, Y. F.: Temperature effect on phase state and reactivity controls atmospheric multiphase chemistry and transport of PAHs, Science Advances, 4, 8, https://doi.org/10.1126/sciadv.aap7314, 2018.

Nam, K. J., Li, Q., Heo, S. K., Tariq, S., Loy-Benitez, J., Woo, T. Y.,Yoo, C. K.: Inter-regional multimedia fate analysis of PAHs and potential risk assessment by integrating deep learning and climate change scenarios, Journal of Hazardous Materials, 411, 12,

776   https://doi.org/10.1016/j.jhazmat.2021.125149, 2021.

777   Octaviani, M., Tost, H.,Lammel, G.: Global simulation of semivolatile organic compounds - development

778   and evaluation of the MESSy submodel SVOC (v1.0), Geoscientific Model Development, 12,

779   3585-3607, https://doi.org/10.5194/gmd-12-3585-2019, 2019.

780   Odabasi, M., Cetin, E.,Sofuoglu, A.: Determination of octanol–air partition coefficients and supercooled

781   liquid vapor pressures of PAHs as a function of temperature: Application to gas–particle

782   partitioning in an urban atmosphere, Atmospheric Environment, 40, 6615-6625,

783   https://doi.org/10.1016/j.atmosenv.2006.05.051, 2006.

784   Quan, J. N., Tie, X. X., Zhang, Q., Liu, Q., Li, X., Gao, Y.,Zhao, D. L.: Characteristics of heavy aerosol

785   pollution during the 2012-2013 winter in Beijing, China, Atmospheric Environment, 88, 83-89,

786   https://doi.org/10.1016/j.atmosenv.2014.01.058, 2014.

787   Ravindra, K., Sokhi, R.,Van Grieken, R.: Atmospheric polycyclic aromatic hydrocarbons: Source

788   attribution, emission factors and regulation, Atmospheric Environment, 42, 2895-2921,

789   https://doi.org/10.1016/j.atmosenv.2007.12.010, 2008.

790   San José, R., Pérez, J. L., Callén, M. S., López, J. M.,Mastral, A.: BaP (PAH) air quality modelling

791   exercise over Zaragoza (Spain) using an adapted version of WRF-CMAQ model,

792   Environmental Pollution, 183, 151-158, https://doi.org/10.1016/j.envpol.2013.02.025, 2013.

793   Seigneur, C., Karamchandani, P., Lohman, K., Vijayaraghavan, K.,Shia, R. L.: Multiscale modeling of

794   the atmospheric fate and transport of mercury, Journal of Geophysical Research-Atmospheres,

795   106, 27795-27809, https://doi.org/10.1029/2000jd000273, 2001.

796   Semeena, V. S.,Lammel, G.: The significance of the grasshopper effect on the atmospheric distribution

797   of   persistent   organic   substances,   Geophysical   Research   Letters,   32,   5,

798   https://doi.org/10.1029/2004gl022229, 2005.

799   Shen, H. Z., Tao, S., Liu, J. F., Huang, Y., Chen, H., Li, W., Zhang, Y. Y., Chen, Y. C., Su, S., Lin, N., Xu,

800   Y. Y., Li, B. G., Wang, X. L.,Liu, W. X.: Global lung cancer risk from PAH exposure highly

801   depends on emission sources and individual susceptibility, Scientific Reports, 4, 8,

802   https://doi.org/10.1038/srep06561, 2014.

803   Shrivastava, M., Lou, S., Zelenyuk, A., Easter, R. C., Corley, R. A., Thrall, B. D., Rasch, P. J., Fast, J. D.,

804   Simonich, S. L. M., Shen, H. Z.,Tao, S.: Global long-range transport and lung cancer risk from

805   polycyclic aromatic hydrocarbons shielded by coatings of organic aerosol, Proceedings of the

806   National Academy of Sciences of the United States of America, 114, 1246-1251,

807   https://doi.org/10.1073/pnas.1618475114, 2017.

808 Skamarock, W. C., Klemp, J. B., Dudhia, J., Gill, D., Barker, D. M., Duda, M. G., Huang, X.-Y., Wang,

809   W.,Powers, J. G. A Description of the Advanced Research WRF Version 3. 2008.

810 Smith, R. L., Davis, J. M.,Speckman, P.: Assessing the human health risk of atmospheric particles,

811   Novartis Found Symp, 220, 59-72; discussion 72-9,

812   https://doi.org/10.1002/9780470515600.ch4, 1999.

813 Stockwell, W. R., Middleton, P., Chang, J. S.,Tang, X. Y.: The Second Generation Regional Acid

814   Deposition Model Chemical Mechanism for Regional Air Quality Modeling, Journal of

815   Geophysical Research-Atmospheres, 95, 16343-16367,

816   https://doi.org/10.1029/JD095iD10p16343, 1990.

817 Strand, A.,Hov, O.: A model strategy for the simulation of chlorinated hydrocarbon distributions in the

818   global environment, Water Air and Soil Pollution, 86, 283-316,

819   https://doi.org/10.1007/bf00279163, 1996.

820 Su, C., Zheng, D. F., Zhang, H.,Liang, R. Y.: The past 40 years' assessment of urban-rural differences in

821   Benzo a pyrene contamination and human health risk in coastal China, Science of the Total

822   Environment, 901, 9, https://doi.org/10.1016/j.scitotenv.2023.165993, 2023.

823 van Noort, P. C. M.: A thermodynamics-based estimation model for adsorption of organic compounds by

824   carbonaceous materials in environmental sorbents, Environmental Toxicology and Chemistry,

825   22, 1179-1188, 2003.

826 Walcek, C. J.,Aleksic, N. M.: A simple but accurate mass conservative, peak-preserving, mixing ratio

827   bounded advection algorithm with Fortran code, Atmospheric Environment, 32, 3863-3880,

828   https://doi.org/10.1016/s1352-2310(98)00099-5, 1998.

829 Wang, L., Zhang, F. Y., Pilot, E., Yu, J., Nie, C. J., Holdaway, J., Yang, L. S., Li, Y. H., Wang, W. Y.,

830   Vardoulakis, S.,Krafft, T.: Taking Action on Air Pollution Control in the Beijing-Tianjin-Hebei

831   (BTH) Region: Progress, Challenges and Opportunities, International Journal of Environmental

832   Research and Public Health, 15, 27, https://doi.org/10.3390/ijerph15020306, 2018.

833 Wang, Y. S., Li, W. J., Gao, W. K., Liu, Z. R., Tian, S. L., Shen, R. R., Ji, D. S., Wang, S., Wang, L. L.,

Tang, G. Q., Song, T., Cheng, M. T., Wang, G. H., Gong, Z. Y., Hao, J. M.,Zhang, Y. H.: Trends in particulate matter and its chemical compositions in China from 2013-2017, Science China-Earth Sciences, 62, 1857-1871, https://doi.org/10.1007/s11430-018-9373-1, 2019.

Wang, Z. F., Maeda, T., Hayashi, M., Hsiao, L. F.,Liu, K. Y.: A nested air quality prediction modeling system for urban and regional scales: Application for high-ozone episode in Taiwan, Water Air and Soil Pollution, 130, 391-396, https://doi.org/10.1023/a:1013833217916, 2001.

Wang, Z. X., Li, J. X., Mu, X., Zhao, L. Y., Gu, C., Gao, H., Ma, J. M., Mao, X. X.,Huang, T.: A WRF-CMAQ modeling of atmospheric PAH cycling and health risks in the heavy petrochemical industrialized Lanzhou valley, Northwest China, Journal of Cleaner Production, 291, 9, https://doi.org/10.1016/j.jclepro.2021.125989, 2021.

Wei, Y., Chen, X. S., Chen, H. S., Li, J., Wang, Z. F., Yang, W. Y., Ge, B. Z., Du, H. Y., Hao, J. Q., Wang, W., Li, J. J., Sun, Y. L.,Huang, H. L.: IAP-AACM v1.0: a global to regional evaluation of the atmospheric chemistry model in CAS-ESM, Atmospheric Chemistry and Physics, 19, 8269-8296, https://doi.org/10.5194/acp-19-8269-2019, 2019.

Wu, Z. C., Chen, X. S., and Wang, Z. F.: A Global-Regional Nested Model of Polycyclic aromatic hydrocarbons, Zenodo [code], https://doi.org/10.5281/zenodo.12214119, 2024.

Wu, Z. C., Chen, X. S., and Wang, Z. F.: Results and validation of Global-Regional Nested Model for polycyclic aromatic hydrocarbons., Zenodo [data set], https://doi.org/10.5281/zenodo.11595165, 2024.

Yan, D. H., Wu, S. H., Zhou, S. L., Tong, G. J., Li, F. F., Wang, Y. M.,Li, B. J.: Characteristics, sources and health risk assessment of airborne particulate PAHs in Chinese cities: A review, Environmental Pollution, 248, 804-814, https://doi.org/10.1016/j.envpol.2019.02.068, 2019.

Yang, L., Zhang, X., Xing, W.L., Zhou, Q.Y., Zhang, L.L., Wu, Q., Zhou, Z.J., Chen, R.J., Toriba, A., Hayakawa, K., Tang, N.: Yearly variation in characteristics and health risk of polycyclic aromatic hydrocarbons and nitro-PAHs in urban shanghai from 2010-2018. Journal of Environmental Sciences, 99, 72-79, https://doi.org/10.1016/j.jes.2020.06.017, 2021.

Ye, Q., Li, J., Chen, X., Chen, H., Yang, W., Du, H., Pan, X., Tang, X., Wang, W., Zhu, L., Li, J., Wang, Z.,Wang, Z.: High-resolution modeling of the distribution of surface air pollutants and their intercontinental transport by a global tropospheric atmospheric chemistry source–receptor

model (GNAQPMS-SM), Geoscientific Model Development, 14, 7573-7604, https://doi.org/10.5194/gmd-14-7573-2021, 2021.

Zaveri, R. A.,Peters, L. K.: A new lumped structure photochemical mechanism for large-scale applications, Journal of Geophysical Research-Atmospheres, 104, 30387-30415, https://doi.org/10.1029/1999jd900876, 1999.

Zhang, H., Zhang, X., Wang, Y., Bai, P.C., Zhang, L.L., Chen, L.J., Han, C., Yang, W.J., Wang, Q.M., Cai, Y.P., Nagao, S., Tang, N.: Factor analysis of recent variations of atmospheric polycyclic aromatic hydrocarbons (PAHs) and 1-nitropyrene (1-NP) in Shenyang, China from 2014 to 2020. Atmospheric Pollution Research, 14, 8, https://doi.org/10.1016/j.apr.2023.101900, 2023.

Zhang, J.W., Feng, L.H., Zhao, Y., Hou, C.C., Gu, Q.: Health risks of PM2.5-bound polycyclic aromatic hydrocarbon (PAH) and heavy metals (PPAH&HM) during the replacement of central heating with urban natural gas in Tianjin, China. Environ. Geochem. Health, 44, 2495-2514, https://doi.org/10.1007/s10653-021-01040-8, 2022.

Zhang, L., Brook, J. R.,Vet, R.: A revised parameterization for gaseous dry deposition in air-quality models, Atmospheric Chemistry and Physics, 3, 2067-2082, https://doi.org/10.5194/acp-3-2067-2003, 2003.

Zhang, M., Xie, J. F., Wang, Z. T., Zhao, L. J., Zhang, H.,Li, M.: Determination and source identification of priority polycyclic aromatic hydrocarbons in PM2.5 in Taiyuan, China, Atmospheric Research, 178, 401-414, https://doi.org/10.1016/j.atmosres.2016.04.005, 2016.

Zhang, Q., Zheng, Y. X., Tong, D., Shao, M., Wang, S. X., Zhang, Y. H., Xu, X. D., Wang, J. N., He, H., Liu, W. Q., Ding, Y. H., Lei, Y., Li, J. H., Wang, Z. F., Zhang, X. Y., Wang, Y. S., Cheng, J., Liu, Y., Shi, Q. R., Yan, L., Geng, G. N., Hong, C. P., Li, M., Liu, F., Zheng, B., Cao, J. J., Ding, A. J., Gao, J., Fu, Q. Y., Huo, J. T., Liu, B. X., Liu, Z. R., Yang, F. M., He, K. B.,Hao, J. M.: Drivers of improved PM2.5 air quality in China from 2013 to 2017, Proceedings of the National Academy of Sciences of the United States of America, 116, 24463-24469, https://doi.org/10.1073/pnas.1907956116, 2019.

Zhang, Y., Hemperly, J., Meskhidze, N.,Skamarock, W. C.: The Global Weather Research and Forecasting (GWRF) Model: Model Evaluation, Sensitivity Study, and Future Year Simulation, Atmospheric and Climate Sciences, 2, 231-253, https://doi.org/10.4236/acs.2012.23024, 2012a.

892 Zhang, Y., Jaeglé, L., van Donkelaar, A., Martin, R. V., Holmes, C. D., Amos, H. M., Wang, Q., Talbot,

893   R., Artz, R., Brooks, S., Luke, W., Holsen, T. M., Felton, D., Miller, E. K., Perry, K. D., Schmeltz,

894   D., Steffen, A., Tordon, R., Weiss-Penzias, P.,Zsolway, R.: Nested-grid simulation of mercury

895   over North America, Atmospheric Chemistry and Physics, 12, 6095-6111,

896   https://doi.org/10.5194/acp-12-6095-2012, 2012b.

897 Zhang, Y., Shen, H., Tao, S.,Ma, J.: Modeling the atmospheric transport and outflow of polycyclic

898   aromatic hydrocarbons emitted from China, Atmospheric Environment, 45, 2820-2827,

899   https://doi.org/10.1016/j.atmosenv.2011.03.006, 2011a.

900 Zhang, Y., Tao, S., Ma, J.,Simonich, S.: Transpacific transport of benzo[a]pyrene emitted from Asia,

901   Atmospheric Chemistry and Physics, 11, 11993-12006, https://doi.org/10.5194/acp-11-11993-

902   2011, 2011b.

903 Zhang, Y. X.,Tao, S.: Global atmospheric emission inventory of polycyclic aromatic hydrocarbons (PAHs)

904   for 2004, Atmospheric Environment, 43, 812-819,

905   https://doi.org/10.1016/j.atmosenv.2008.10.050, 2009.

906 Zhang, Y. X., Tao, S., Shen, H. Z.,Ma, J. M.: Inhalation exposure to ambient polycyclic aromatic

907   hydrocarbons and lung cancer risk of Chinese population, Proceedings of the National Academy

908   of Sciences of the United States of America, 106, 21063-21067,

909   https://doi.org/10.1073/pnas.0905756106, 2009.

910 Zhen, Z. X.: Observation and simulation of atmospheric polycyclic aromatic hydrocarbons in the North

911   China Plain, Ph.D.thesis, Nanjing university of information science and technology, China, 142

912   pp., 2023.

913 Zhu, F. J., Ma, W. L., Hu, P. T., Zhang, Z. F.,Li, Y. F.: Temporal trends of atmospheric PAHs: Implications

914   for the influence of the clean air action, Journal of Cleaner Production, 296, 8,

915   https://doi.org/10.1016/j.jclepro.2021.126494, 2021.